Abstract

One of the most active research topics in physics at the moment is the nature of dark matter (DM). Many current theories provide viable candidates for DM most notably in the form of weakly interacting massive particles (WIMPs). One such theory is universal extra dimensions (UED) which provides the so-called lightest Kaluza-Klein particle (LKP) as a stable particle. In the simplest theory of UED, minimal UED, the first Kaluza-Klein excitation of the photon takes the role of the LKP and is in fact a typical WIMP. In this thesis the direct detection cross sections of the KK-photon are calculated. This was done by implementing the direct detection part of the UED module in DarkSUSY, a FORTRAN package for calculating DM observables. The cross sections were found to satisfy the experimental bounds for values of the LKP mass above 450 GeV.

Contents

1 Introduction

The dark matter problem is one of the largest open problems in physics as of today. The standard model of particle physics can only account for less than 25 % of the matter content of the universe. The rest must be attributed to some new form of matter called "dark matter" (DM). As of today the general consensus among physicists is that DM is explained by introducing some new particle(s) in addition to the standard model particles. The most promising DM candidates are weakly interacting massive particles (WIMPs) which naturally occur in several different theories proposed to solve problems unrelated to DM.

One example of a theory which predicts a WIMP as a possible solution to the DM problem is universal extra dimensions (UED). UED postulates the existence of one (or more) extra dimension(s) which all standard model particles can freely propagate in. In order to explain why this extra dimension has not been discovered yet it has to be compacted on a sufficiently small scale. As the standard model particles are allowed to propagate in the extra dimension they will have a momentum component which is not seen by a 3D observer, which must be interpreted as an extra mass term. Thus every standard model particle will be accompanied by a "tower" of Kaluza-Klein (KK-)particles which are identical to in all regards except the mass. By the symmetries of the extra dimension the lightest KK-particle (LKP) is stable, and a viable candidate for DM.

The goal of this thesis has been to calculate the the elastic scattering cross sections between the DM candidate being the KK-photon, in order to check whether UED is or will excluded as a solution to the DM problem by current or future direct detection experiments. the so-called direct detection experiments look for events where DM has scattered of atomic nuclei in order to probe the elastic scattering cross section with nuclei. In general direct detection experiments have placed strict bounds on the parameter space of WIMPs. These cross sections have been calculated before, however recently new contributions to the radiative corrections in minimal UED have calculated by Freitas et. al. [23]. As the new corrections may have a large impact on the cross sections it is important to include them. Furthermore the impact of the gluon content of the nucleon has for the first time been given the appropriate treatment. The cross sections have been calculated numerically by implementing the expressions found here in DarkSUSY [14].

The outline of this thesis is as follows chapter 2 introduces the most important extra dimensional concepts and the field content of UED. It is assumed the reader has some familiarity with quantum field theory and electroweak symmetry breaking. Chapter 3 motivates the existence of DM and the validity of the KK-photon as a DM candidate. This is done by giving a brief overview of some experimental evidence as well as a justification of the KK-photon as the DM candidate. Finally it will give a brief introduction to direct detection experiments. Chapter 4 presents the calculation of the effective four-point couplings needed for the elastic scattering cross section. Chapter 5 presents the cross sections found using DarkSUSY. This includes the cross sections in minnial UED as well as a phenomenological approach where the masses of KK-quarks are treated as free parameters. Chapter 6 will compare the results to the current and projected experimental bounds from the XENON collaborrations [9].

2 Universal extra dimensions

The idea of including one or more extra dimension (ED) in addition to the three spacial and one temporal we are used to was first studied in the early 20-th century by Nordström, Kaluza and

Klein [33] [35], in an attempt to unify gravity and electromagnetism. The fact no ED has been detected tells us they must be so small the energies associated with them are too large to be detected by current experiments. These bounds will depend on the nature of the ED and which fields are allowed to propagate there. If only gravity is affected by the extra dimension this the upper bound on this dimension is $218\mu m$ [29]. If instead all fields are allowed tho propagate in the fifth dimension the bound is at $R^{-1} > 1.4$ TeV based on LHC searches [11].

2.1 Kaluza-Klein theory

In 1921 Kaluza [33] proposed a purely classical 5 Dimensional version of Einstein's theory of general relativity. Uppercase latin indices $M, N = 0, 1, 2, 3, 5$ will here denote the 5 space-time dimensions while the regular 4 space-time dimes ions will be denoted by the usual $\mu, \nu = 0, 1, 2, 3$ and lowercase latin indices $i, j = 1, 2, 3$ being used for 3 spacial dimensions. The 5D metric

$$g_{MN} = \begin{pmatrix} g_{\mu\nu} + \chi^2 A_\mu A_\nu & \chi^2 A_\mu \\ \chi^2 A_\nu & \chi^2 \end{pmatrix} \tag{1}$$

contains the 4D metric $g_{\mu\nu}$ as well as a 4-vector A_μ, which can be associated with the electromagnetic vector-potential and a scalar χ. Kaluza also introduced what he called the "cylinder condition": all derivatives of the 5D metric with respect to the 5th coordinate can be neglected.

With this ansatz the 5D versions of Einstein's equations reduced to the 4D Einstein's equations and Maxwell's equation and an equation for the scalar field χ. In 1926 Klein suggested compactification on as an explanation for the cylinder condition [35]. The idea of compactification on a circle $\mathbf{S}^1$ can be realized by making the 5th dimension closed and periodic. This can be visualised as the surface of a cylinder where the height should be considered as the uncompactified dimensions, in this case the 4 regular space-time dimension, and the circumference should be considered as the compactified dimension. If the radius of this cylinder is small enough it will from a distance look one dimensional, but up close it will clearly be 2 dimensional.

Let us consider a scalar field $\phi(x^\mu, y)$ which is allowed to propagate in 5D. We take the 5th dimension to be compactified on a scale R by imposing the condition

$$y \sim y + 2\pi R\,, \tag{2}$$

This gives every field periodic boundary conditions allowing the Fourier decomposition in of any field the y-direction.

$$\phi(x, y) = \frac{1}{\sqrt{2\pi R}} \sum_n \phi^{(n)}(x) e^{-i\frac{n}{R}y} \tag{3}$$

The 5D field ϕ satisfies the 5D Klein-Gordon (K-G) equation in flat space-time

$$(\Box^{(5)} + m^2)\phi = (\Box^{(4)} - \partial_y^2 + m^2) \sum_n \phi^{(n)}(x) e^{-i\frac{n}{R}y} = 0\,, \tag{4}$$

This gives the condition on the Fourier components $\phi^{(n)}(x)$

$$(\Box^{(4)} + (\frac{n}{R})^2 + m^2)\phi^{(n)}(x) = 0\,. \tag{5}$$

the Fourier components satisfies the K-G equation in 4D with a mass $m_n^2 = m^2 + \frac{n^2}{R^2}$. Therefore a particle propagating in 5D with mass m is equivalent to an infinite "tower" of Kaluza-Klein (KK)

particles with mass m_n in the effective 4D theory. A similar treatment of fermionic fields gives a tower of particles with mass $m_n = m + \frac{n}{R}$

The appearance of this tower of massive states can also be understood qualitatively as follows. A particle propagating in 5D will have a "5-momentum" p^M which consists of the 4-momentum in the 4 regular dimensions p^μ and the momentum in the fifth dimension p^y. From the perspective of the effective 4D theory we do not see this momentum p^y however it's contribution to the (kinetic) energy of the particle is simply understood as a mass.

If the y-direction is translationally invariant, that is a coordinate transformation along the y-direction does not affect the physics, we know from Noether's theorem that the momentum in the y-direction should be conserved which in the 4D theory means the KK-number n is conserved.

2.2 Orbifold compactification

The simplest approach to a compactified ED-theory, described in the previous section has two major problems. The first problem being that it predicts additional massless scalar degrees of freedom which have not been observed experimentally, as the 5th component of the 5D vectorfields transform as scalars under 4D Lorentz transformations. The second problem is that chiral fermions can not exist in an odd number of dimensions.

One solution to both problems is to compactify on an orbifold ($S^1/\mathbb{Z}_2$) instead of a circle. Which has a mirror-symmetry under orbifold projection $y \to -y$. Together with Eq.(2) this gives a total symmetry:

$$y \sim 2\pi R - y\,, \tag{6}$$

The orbifold can be understood as a line segment $[0, \pi R]$ where traveling straight along this line segment one would bounce back upon reaching one of the orbifold fixed points (edges).

Under orbifold projections fields transform either even $P_{\mathbb{Z}_2}\phi(x,y) = \phi(x,-y)$ or odd $P_{\mathbb{Z}_2}\phi(x,y) = -\phi(x,-y)$ as such their respective Fourier decompositions are:

$$\phi_{even}(x,y) = \frac{1}{\sqrt{2\pi R}}\phi^{(0)}_{even}(x) + \frac{1}{\sqrt{\pi R}}\sum_n \phi^{(n)}_{even}(x)\cos\left(\frac{ny}{R}\right) \tag{7}$$

$$\phi_{odd}(x,y) = \frac{1}{\sqrt{\pi R}}\sum_n \phi^{(n)}_{odd}(x)\sin\left(\frac{ny}{R}\right) \tag{8}$$

As only even fields have zero-modes we can get rid of the additional light scalars by demanding they transform odd under orbifold transformations.

This compactification scheme does not fully preserve translational symmetry in the y-direction, however there is still a symmetry under translations by πR which give rise to the conserved quantity KK-parity given by $(-1)^n$ where n is the KK-number. This follows from the Fourier expansion as:

$$\cos\left(\frac{n(y+\pi R)}{R}\right) = (-1)^n\cos\left(\frac{ny}{R}\right), \tag{9}$$

$$\sin\left(\frac{n(y+\pi R)}{R}\right) = (-1)^n\sin\left(\frac{ny}{R}\right), \tag{10}$$

This means any interaction between a particle with KK-number 1 and a particle with KK-number 0, a standard model (SM) particle, needs to result in one particle with KK-number 1. As a result the Lightest KK-particle (LKP), that is the lightest particle with $n = 1$, is stable.

2.3 The standard model in 5D

The model of universal extra dimensions (UED) [4] is essentially the higher dimensional version of the standard model.

As in the SM the Lagrangian, before electro-weak symmetry breaking, can be constructed by adding all terms allowed by Lorentz invariance and local gauge invariance under the SM gauge group

$$G_{SM} = SU(3) \times SU(2)_L \times U(1)_Y \,. \tag{11}$$

As the Lagrangian is a local function only sensitive to the local geometry, not the topology, the only difference between the 4D standard model and the standard model in our UED scenario is the number of (space-like) coordinates. We can therefore state the Lagrangian

$$\hat{\mathcal{L}} = -\frac{1}{4} F^r_{MN} F^{rMN} + i\bar{\psi}\not{D}\psi + \psi_i \lambda_{ij} \psi_j + h.c. + |D_M \phi|^2 - V(\phi) \,. \tag{12}$$

In order to preserve gauge invariance under G_{SM} we need to introduce the covariant derivative

$$D_M = \partial_M - i\hat{g}_s G^a_M t^a - i\hat{g} A^b_M t^b - iY\hat{g}_Y B_M \,. \tag{13}$$

In order to study the low energy regime of a UED-theory, it is convenient to express it as an effective 4D theory. This is done by integrating out the 5th dimension with the help of the expansions Eq. 7 and 8 and then identifying the zero-modes as the SM fields. One finds the effective 4D gauge couplings, i.e. the ones we measure, related to the 5D ones by

$$g = \frac{\hat{g}}{\sqrt{2\pi R}} \,. \tag{14}$$

As the 4D couplings are dimensionless, the 5D coupling have mass dimension $-\frac{1}{2}$, hence the theory is non-renormalizable and should be considered as an effective theory only valid up to some cutoff Λ.

2.4 Radiative corrections

Radiative corrections appear in perturbative theories as corrections to masses and couplings. Radiative mass corrections arise from higher order corrections to two-point correlation functions. These are calculated by adding all possible diagrams with one incoming and one outgoing particle. To leading order the two point correlation functions is just the Feynman propagator.

The sum over all such diagrams evaluates to

$$\langle \Omega | \, \phi(p)\phi(p) \, | \Omega \rangle = \frac{i}{p^2 - m_0^2 - M^2(p^2)} \,, \tag{15}$$

where m_0 is the bare mass of the particle and $M(p^2)$ is calculated from the diagrams. Specifically $-iM^2(p^2)$ is the sum of all one-particle-irreducible insertions into the propagator [39]. Therefore the higher order corrections to the two-point correlation function can be realized by using a mass $m^2(p^2) = m_0^2 + M^2(p^2)$ in the propagator when computing diagrams, as any experiment measures the full process not just the leading approximation we have to identify m as the mass we measure.

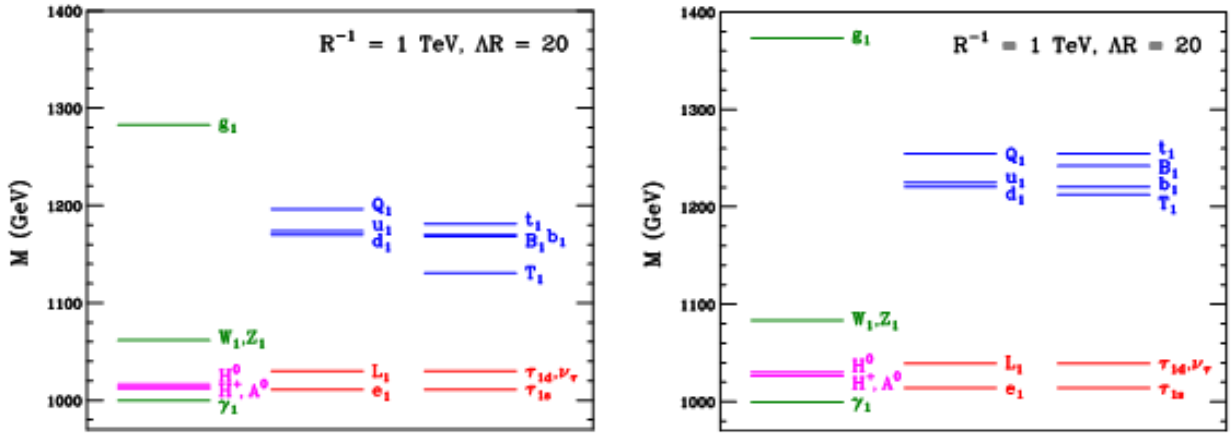

Figure 1: (Taken from [23]) mass specurum at R^{-1} = 1 TeV and ΛR = 20 without (left) and with (right) finite corrections

In UED mass corrections to the compactification mass term can be split into two contributions: bulk corrections and boundary corrections. One way of isolating the corrections due to the EDs is by subtracting every (formally infinite) diagram in the compactified theory from the equivalent diagram in the uncompactified 4D theory [23]. All divergences present in the (renormailizable) 4D theory will then cancel and leave a well defined mass shift δm^2 which is purely due to the extra dimension.

The compactification on $\mathbf{S}^1$ does not break Lorentz invariance locally, but globally which gives rise to bulk corrections. These corrections are due to diagrams with an internal loop winding around the extra dimension. The corrections are finite and well defined as the loops can not be smaller than the extra dimension.

Boundary corrections are a consequence of orbifolding, as translational invariance is broken at the boundary of the orbifold which introduces new terms in the Lagrangian localized at the boundary. In order to obtain these corrections one must calculate the relevant loop diagrams using modified propagators obtained by writing the field in terms of an unconstrained field [25]. These corrections are log divergent as the loop diagrams involve integrals of the form $\int \frac{d^4q}{(2\pi)^4} \frac{1}{(q^2-m_1^2)((q-p)^2-m_2^2)}$. One way of addressing this divergence is by introducing a cut-off scale Λ above which the theory should not be considered valid. This means the previously infinite term is replaced by $\ln(\Lambda)$. This introduces a dependence on Λ to the radiative corrections and in turn the masses.

In minimal UED (mUED) KK-number is assumed to be be approximately conserved which means divergent boundary terms are negligible. MUED is completely described by 2 free parameters R and Λ which makes the theory appealing from a phenomenological standpoint. For more general UED cases however the boundary terms might violate conservation of KK-number. In these cases the radiative corrections would be different from the mUED case and might depend on other parameters. As such a more phenomenological approach of taking the radiative corrections themselves, or equivalently the masses, as free parameters.

In 2018 Freitas, Kong and Wiegand published an article [23] where the finite corrections in mUED were calculated. Before this only terms proportional to $\ln(\Lambda R)$ were computed [17]. In order to avoid regimes where the theory becomes non-penetrative the cutoff ΛR is typically assumed to be in the range 20-50[12]. In this range the logarithms are small enough that non-logarithmic contributions may be significant. As the mass contribution originating from compactification $\frac{n}{R}$ is significantly larger than any electroweak mass all KK-modes will be approximately degenerate, with the exception of the top-quark. Radiative mass corrections help lifting this degeneracy and are therefore phenomenologically important.

2.5 Gauge fields

As the gauge fields of the standard model are all massless before electro-weak symmetry breaking the first 4 components A_μ need to have zero-modes, hence they must transform even. It then follows from gauge invarinace

$$A_\mu(x,y) = A_\mu(x,-y) \sim A_\mu(x,y) + \partial_\mu\theta(x,y)\,. \tag{16}$$

The gauge-functions θ must transform even, thus $\partial_y\theta(x,y)$ transforms odd which means A_5 must transform odd. This is also needed as the zero mode of A_5 transforms as a scalar under 4D Lorentz transformations and thus would appear as a light scalar, which is not observed.

The kinetic 5D Lagrangian for a gauge-field reads:

$$\hat{\mathcal{L}}_{guage} = -\frac{1}{4}F^r_{MN}F^{rMN}\,, \tag{17}$$

with U(1) field strength tensor:

$$F_{MN} = \partial_M B_N - \partial_N B_M\,, \tag{18}$$

or SU(2) field strength tensor:

$$F^r_{MN} = \partial_M A^r_N - \partial_N A^r_M + \hat{g}\epsilon^{rst}A^s_M A^t_N\,. \tag{19}$$

In order to get the 4D theory we need to integrate out the internal degrees of freedom. This can be easily done by inserting the appropriate expansion, based on the above discussion of odd/even components these are:

$$\begin{aligned} A_\mu(x,y) &= \frac{1}{\sqrt{2\pi R}}A^{(0)}_\mu(x) + \sum_{n=1}^{\infty}\frac{1}{\sqrt{\pi R}}A^{(n)}_\mu(x)\cos\left(\frac{ny}{R}\right), \\ A_5(x,y) &= \sum_{n=1}^{\infty}\frac{1}{\sqrt{\pi R}}A^{(n)}_\mu(x)\sin\left(\frac{ny}{R}\right). \end{aligned} \tag{20}$$

For a U(1) gauge field the kinetic part of the Lagrangian then becomes:

$$\begin{aligned} \mathcal{L}_{guage} &= \int_0^{2\pi R} dy - \frac{1}{4}(\partial_M A_N - \partial_N A_M)(\partial^M A^N - \partial^N A^M) \\ &= -\frac{1}{4}\sum_{n=0}^{\infty}(\partial_\mu A^{(n)}_\nu - \partial_\nu A^{(n)}_\mu)(\partial^\mu A^{(n)\nu} - \partial^\nu A^{(n)\mu}) \end{aligned}$$

$$-\frac{1}{4}\sum_{n=1}^{\infty}(\partial_\mu A_5^{(n)}+\frac{n}{R}A_\mu^{(n)})(\partial^\mu A^{(n)5}-\frac{n}{R}A^{(n)\mu})\,, \tag{21}$$

this result also holds for the kinetic terms of other gauge fields.

A massless vector in 5D has 3 degrees of freedom, which is the same as a 4D massive vector. Meaning that there are no degrees of freedom left for the scalar A_5 which means that it should not be considered a physical field. This can also be seen by the fact they can be removed from the Lagrangian by the gauge fixing condition $\theta = -\frac{R}{n}A_5$ in eq.16. We can therefore interpret it as the Goldstone Boson that's eaten by the KK-modes to give them the mass-term. This gives us a mechanism of giving a gauge-field a mass-term which is independent of the Higgs mechanism.

2.6 Fermions

Before specializing to 5D UED lets look at spinors in d dimensions. As in the 4D case the Dirac matrices are defined by the Clifford algebra:

$$\{\Gamma^M,\Gamma^N\} = 2g^{MN}\,. \tag{22}$$

In the case where d is even we can use $2^{\frac{d}{2}}\times 2^{\frac{d}{2}}$ matrices constructed from the matrices in $d-2$ dimensions [40].

For odd d take the Dirac matrices in dimension $d-1$ and add

$$\Gamma = i^{\frac{d-1}{2}}\Gamma^0\Gamma^1...\Gamma^{d-2}\,. \tag{23}$$

We now have a set of d Dirac matrices which can be used to construct a set of matrices:

$$\Sigma^{MN} = \frac{i}{4}[\Gamma^M,\Gamma^N]\,, \tag{24}$$

which satisfy the Lorentz algebra:

$$[\Sigma^{MN},\Sigma^{RS}] = i(g^{NR}\Sigma^{MS}-g^{MR}\Sigma^{NS}+g^{MS}\Sigma^{NR}-g^{NS}\Sigma^{MS})\,. \tag{25}$$

The Dirac representation is then the vector space spanned by spinors $s = (s_0, s_1, ..., s_{\lfloor\frac{d}{2}\rfloor})$ where s_a are the eigenvalues of

$$S_a = \Gamma^{a+}\Gamma^{a-}-\frac{1}{2}\,, \tag{26}$$

where the raising and lowering operators are defined as

$$\Gamma^{0\pm} = \frac{i}{2}(\pm\Gamma^0+\Gamma^1)\,, \tag{27}$$

$$\Gamma^{a\pm} = \frac{i}{2}(\Gamma^{2a}\pm i\Gamma^{2a+1}) \text{ for } a = 1,2,..,\left\lfloor\frac{d}{2}\right\rfloor.$$

In odd dimensions this representation is an irreducible ($2^{\frac{d-1}{2}}$-dim) representation of the Lorentz algebra. However in even dimensions there exists a matrix defined by Eq.23 which (anti-) commutes with every (Γ^M) Σ^{MN}, hence eigenvectors of Γ with different eigenvalues do not mix under

Lorentz-transformations. The ($2^{\frac{d}{2}}$-dim) Dirac representation can be reduced to two distinct ($2^{\frac{d}{2}-1}$-dim) Weyl representations which only act on the subspace corresponding to the chirality $\Gamma s = \pm s$. We can construct projection operators:

$$P_{R/L} = \frac{1}{2}(1 \pm \Gamma)\,, \tag{28}$$

which allows us to project out chiral states $P_{R/L}\psi = \psi_{R/L}$.

Let us now specialize to 5D where we can take the usual 4D Dirac matrices and add the usual chirality operator

$$\gamma^5 = i\gamma^0\gamma^1\gamma^2\gamma^3\,, \tag{29}$$

as the fifth Dirac matrix. Strictly speaking we should use $\Gamma^5 = i\gamma^5$ as 22 implies $(\Gamma^5)^2 = -1$ where as the usual 4D chirality operator squares to 1. From now on Γ will denote a 5D Dirac matrices where as γ will denote a 4D ones if the distinction is necessary. Under 5D Lorentz transformations right- and left-handed spinors will mix as the chirality operator is part of the Lorentz algebra. Under 4D Lorentz transformation however they do not mix and we may therefore assign different orbifold transformations to them and recover the SM at zero mode level where we have a singlet ψ_s and a doublet ψ_d of definite chirality states:

$$\begin{aligned}
\psi_d &= \frac{1}{\sqrt{2\pi R}}\psi_{dL}^{(0)} + \frac{1}{\sqrt{\pi R}}\sum_{n=1}^{\infty}(\psi_{dL}^{(n)}\cos\left(\frac{ny}{R}\right) + \psi_{sR}^{(n)}\sin\left(\frac{ny}{R}\right))\,,\\
\psi_s &= \frac{1}{\sqrt{2\pi R}}\psi_{sR}^{(0)} + \frac{1}{\sqrt{\pi R}}\sum_{n=1}^{\infty}(\psi_{sR}^{(n)}\cos\left(\frac{ny}{R}\right) + \psi_{dL}^{(n)}\sin\left(\frac{ny}{R}\right))\,.
\end{aligned} \tag{30}$$

We can now integrate out the 5th dimension just like we did for gauge fields. Including a mass term from the electro-weak symmetry-breaking which will be discussed in the next section we get:

$$\begin{aligned}
\mathcal{L}_{fermion} &= \int_0^{2\pi R} dy i\bar{\psi}_d\Gamma^M D_M\psi_d + i\bar{\psi}_s\Gamma^M D_M\psi_s - m_{EW}(\bar{\psi}_d\psi_s + \bar{\psi}_s\psi_d)\\
&= \bar{\psi}^{(0)}(i\not{D} - m_{EW})\psi^{(0)} + \sum_{n=1}^{\infty}\bar{\xi}_s^{(n)}(i\not{D} - m_n)\xi_s^{(n)} + \sum_{n=1}^{\infty}\bar{\xi}_d^{(n)}(i\not{D} - m_n)\xi_d^{(n)}\,,
\end{aligned} \tag{31}$$

where the fermion states have been redefined in terms of the mass eigenstates which are

$$\begin{aligned}
\xi_d &= \psi_d^{(n)}\cos\left(\alpha^{(n)}\right) + \psi_s^{(n)}\sin\left(\alpha^{(n)}\right)\,,\\
\xi_s &= -\psi_s^{(n)}\gamma^5\cos\left(\alpha^{(n)}\right) + \psi_d^{(n)}\gamma^5\sin\left(\alpha^{(n)}\right)\,,
\end{aligned} \tag{32}$$

with mixing angle

$$\tan(2\alpha) = \frac{2m_{EW}}{2\frac{n}{R} + \delta m_s + \delta m_d}\,. \tag{33}$$

2.7 The Higgs mechanism

From the principle of gauge invariance it follows that no gauge boson or fermion can have an explicit mass term. As SM particles do indeed have a mass we need some way of generating a mass-term without violating gauge invarince. This is achived by the electroweak symmetry breaking.

The Higgs field is a complex SU(2)-doublet

$$\phi = \frac{1}{\sqrt{2}} \begin{pmatrix} \chi^2 + i\chi^1 \\ H - i\chi^3 \end{pmatrix}. \tag{34}$$

The 5D Higgs Lagrangian is given as:

$$\hat{\mathcal{L}}_{higgs} = (D_M \phi)^\dagger (D^M \phi) - V(\phi), \tag{35}$$

with a potential

$$V(\phi) = -\mu^2 \phi^\dagger \phi + \lambda (\phi^\dagger \phi)^2. \tag{36}$$

This potential has a minimum at $|\phi| = v = \sqrt{\frac{\mu^2}{\lambda}}$, which should therefore be considered the true vacuum of the theory. We therefor making the replacement $H \to H + v$, which introduces mass terms for gauge bosons.

In order to cancel cross-terms mixing scalar and vector fields we add gauge-fixing terms to the Lagrangian[13]

$$\hat{\mathcal{L}}_{gaugefix} = -\frac{1}{2} \sum_i (\mathcal{G}^i)^2 - \frac{1}{2} (\mathcal{G}^Y)^2, \tag{37}$$

$$\mathcal{G}^i = \frac{1}{\sqrt{\xi}} (\partial^\mu A^i_\mu - \xi(-m_w \chi^i + \partial_5 A^i_5)),$$

$$\mathcal{G}^Y = \frac{1}{\sqrt{\xi}} (\partial^\mu B_\mu - \xi(s_w m_w Z\chi^3 + \partial_5 B_5)). \tag{38}$$

The mass eigenstates will then be the 5D version of the usual vectors of the Glashow-Weinberg-Salam theory

$$W_M = \frac{1}{\sqrt{2}} (A^1_M \mp i A^2_M),$$

$$A_M = \sin(\hat{\theta}_w) A^3_M + \cos(\hat{\theta}_w) B_M,$$

$$Z_M = \cos(\hat{\theta}_w) A^3_M - \sin(\hat{\theta}_w) B_M, \tag{39}$$

With the weak mixing angel given by

$$\sin(\hat{\theta}_w) = \frac{\hat{g}_Y}{\sqrt{\hat{g}_Y^2 + \hat{g}^2}}, \qquad \cos(\hat{\theta}_w) = \frac{\hat{g}}{\sqrt{\hat{g}_Y^2 + \hat{g}^2}}. \tag{40}$$

Finally we can integrate out the 5th dimension, and find that the mixing angle at higher KK-level is given by:

$$\tan\left(2\theta_w^{(n)}\right) = \frac{v^2 g_Y g}{\frac{1}{2}v^2(g_Y^2 - g^2) + 2\delta m^2_{B^{(n)}} - 2\delta m^2_{A^{3(n)}}}. \tag{41}$$

Typically $2\delta m^2_{B^{(n)}} - 2\delta m^2_{A^{3(n)}} \gg v^2(g_Y^2 - g^2)$ meaning that the mixing angles for higher modes will be significantly smaller than the SM mixing angles which implies that the KK-photon is well approximated by $B^{(1)}$

The mass eigenstates of scalars given by:

$$\begin{aligned}
a_0^{(n)} &= \frac{n}{RM_Z^{(n)}}\chi^{3(n)} + \frac{m_z}{M_Z^{(n)}}Z_5^{(n)} \\
G_0^{(n)} &= \frac{m_z}{M_Z^{(n)}}\chi^{3(n)} - \frac{n}{RM_Z^{(n)}}Z_5^{(n)} \\
a_\pm^{(n)} &= \frac{n}{RM_W^{(n)}}\chi^{\pm(n)} + \frac{m_W}{M_W^{(n)}}W_5^{\pm(n)} \\
G_\pm^{(n)} &= \frac{m_W}{M_W^{(n)}}\chi^{\pm(n)} - \frac{n}{RM_W^{(n)}}W_5^{\pm(n)}
\end{aligned} \tag{42}$$

Where $m_{z/w}$ is the mass given by electroweak symmetry breaking in the standard model and $M^{(n)}_{Z/W} = \sqrt{\frac{n^2}{R^2} + m^2_{Z/W}}$.

The Goldstone bosons $A_5^{(n)}, G_0^{(n)}$ and $G_\pm^{(n)}$ can all be removed by adopting unitary gauge $\xi \to \infty$

Before electroweak symmetry breaking at zero-mode level we have 4 massless vectors A^i_μ, B_μ each with 2 degrees of freedom (d.o.f) and one complex scalar SU(2)-doublet ϕ with 4 d.o.f. After electroweak symmetry breaking at zero-mode level we have 3 massive vectors each with 3 d.o.f, 1 massless vector γ_μ with 2 d.o.f and one real scalar H with 1 d.o.f. This gives 12 d.o.f in total both before and after symmetry breaking.

At the higher KK-levels there are 2 distinct mechanisms for generating masses, the KK-mechanism itself, explained in section 2.2, and electroweak symmetry breaking. Before electroweak symmetry breaking we have 4 massless vectors $A^{i(n)}_\mu, B^{(n)}_\mu$ each with 2 d.o.f, 4 massless scalars $A_5^{i(n)}, B_5^{(n)}$ each contributing 1 d.o.f and 1 complex scalar $\phi^{(n)}$ with 4 d.o.f. The use of the term mass less is justified here as one should consider the 5-th component of the vector as the Goldstone boson giving mass to the vector. As such if we were to consider them massive, which would mean they each have 3 d.o.f, we should not count the fifth components as physical d.o.f.

After electroweak symmetry breaking we have 4 scalars $a_0^{(n)}, a_\pm^{(n)}, H(n)$ each with 1 d.o.f and 4 massive vectors each with 3 d.o.f. Both before and after electroweak symmetry breaking we have a total of 16 d.o.f.

All SM- fermions except the neutrinos are massive. In order to generate a fermion mass term we need to include a gauge invariant term which couples the relevant fermion to the Higgs field. The only possible such term is

$$\hat{\mathcal{L}}_{Yukawa} = -\hat{\lambda}_D(\bar{\psi}_d^U, \bar{\psi}_d^D)\cdot\phi\psi_s^D - \hat{\lambda}_U(\bar{\psi}_d^U, \bar{\psi}_d^D)\cdot\phi\psi_s^U + h.c. \tag{43}$$

The U/D index denoting the weak isospin of the fermion, up-type quarks and neutrinos having $T^3 = +\frac{1}{2}$ and down-type quarks and charged leptons having $T^3 = -\frac{1}{2}$. Preforming the same shift $H \to H + v$ we find the fermion mass $m_{EW} = \frac{\lambda v}{\sqrt{2}}$.

3 Dark matter

One of the great successes of cosmology was that by measuring the cosmic microwave background (CMB) we determine exactly what the universe is made of. The latest such measurements was done by the Planck collaboration [2]. Finally we could answer the question: "what is the universe made of?" the answer turns out to be: for the most part we don't know. About 68% of the energy content is due a contribution called dark energy, which is well modeled by Einsteins cosmological constant however the origin of this contribution is a mystery. Luminous matter, i.e. the visible matter in stars, galaxies and such make up less than 1 % and baryonic matter, i.e. the matter in the standard model, makes up about 4%. This leaves the last 27% which must be made of some form of matter arising from yet unknown physics referred to as dark matter (DM). The most accepted solution as of today is to introduce some new particle(s) in addition to the standard model.

3.1 Experimental evidence for Dark Matter

The CMB gives the most precise measurement of DM of $\Omega_{CDM}h^2 \approx 0.120 \pm 0.001$ [2]. $\Omega_{CDM} = \frac{\rho_{CDM}}{\rho_{crit}}$ is the ration between the energy density of cold DM and the critical density, the density required for a flat universe. While the CMB is the most precise measurement of the DM density it is not the only evidence of DM some other are:

Rotation curves

According to Newtonian mechanics a star at distance r from the center of the galaxy should be orbiting with a velocity $v(r) = \sqrt{\frac{GM(r)}{r}}$ where $M(r)$ is the mass enclosed by the orbit. In 1970 [46] Rubin and Ford found the velocities of stars in the Andromeda galaxy to be constant for large r which suggests that the mass density of the galaxy scales as $\rho(r) \propto r^{-2}$. This does not agree with the density of luminous matter suggesting that there must be DM present. Similar measurements of other galaxies have also indicated dark matter dominates (almost) all galaxies.

Structure formation

Dark matter is also needed to explain the formation of large scale structures. These structures were formed from density perturbations in the early universe, regions with slight over-densities would attract more matter gravitationally causing the over-density to grow. This effect would be counteracted by radiation and the expansion of the universe. DM however is not affected by radiation and thus would only have to overcome the expansion of the universe for over-densities to grow [18].

Gravitational lensing

One of the consequences of general relativity is that light is deflected by the gravitational field, the deflection angle is larger in stronger fields. In order to explain the impact galaxies and clusters have on lensing DM must be introduced [36]. By measuring the distortion of objects in the night sky independent evidence for DM has been discovered at all scales.

3.2 Weakly interacting massive particles and relic density

The most promising candidates for dark matter are weakly interacting massive particles (WIMPs). These are particles with mass 100 GeV-$\mathcal{O}(TeV)$ which as the name suggest interact weakly. WIMPs appear in many extensions to the SM, such as supersymmetry and UED. The main reason why WIMPs are so promising is "the WIMP miracle".

If we take all DM to consist of WIMPs the abundance can be explained by thermal freeze-out. In the early universe WIMPs and SM particles existed in thermal equilibrium. However as the universe cooled the expansion rate became significantly larger than the interaction rate and the WIMP density became approximately constant in the comoving frame. This gives a method for predicting the density left over from the early univerese, the relic density, of a given WIMP.

The time evolution of the number density n of DM or any other particle is given by the Boltzmann equation [19]:

$$\frac{dn}{dt} + 3Hn = -\langle \sigma v \rangle (n^2 - n_{eq}^2) \tag{44}$$

Where the term involving the Hubble parameter H accounts for dilution due to the expansion of the universe. $\langle \sigma v \rangle$ denotes the thermal average over the annihilation cross section times the relative velocities of the particles. For a non-relativistic particle the equilibrium density is given by the Maxwell-Boltzmann distribution:

$$n_{eq} = g(\frac{mT}{2\pi})^{\frac{3}{2}} e^{-\frac{m}{T}} . \tag{45}$$

If there does not exist any other particles with a mass close to the DM candidate a good estimate for the relic density today is given by[31]:

$$\Omega_{CDM} h^2 \sim \frac{3 \cdot 10^{-27} c m^3 s^{-1}}{\langle \sigma v \rangle} , \tag{46}$$

where h is the Hubble constant in units of 100 $kms^{-1}Mpc^{-1}$.

The annihilation cross section of a WIMP can be estimated as $\sigma v \sim \frac{g^4}{m_\chi^2}$, g being the SU(2) coupling constant. Based on this we can use the measured relic density to estimate what mass gives the right relic density which turns out to be in the range 100 GeV-$\mathcal{O}(TeV)$ which is already the natural mass range for WIMPs. The WIMP miracle refers to the fact that WIMPs predicted by theories attempting to solve unrelated problems accidentally predicted a relic density which agreed well with the observed DM density.

If however the DM candidate is accompanied by other particles with a similar mass, like for example in UED, one has to consider the effect of co-annihilations, which may give large corrections to Eq.46. Co-annihilations are processes where the DM candidate annihilates with another

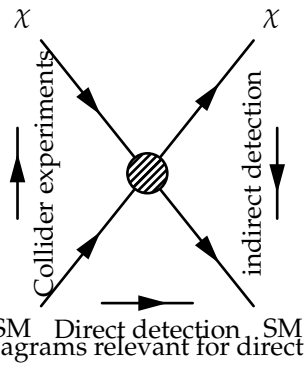

Figure 2: Schematic diagrams relevant for direct and indirect detection

particle leaving only SM particles. The Boltzmann equation **??**

$$\frac{dn}{dt} + 3Hn = -\sum_{i,j} \left\langle \sigma_{ij} v \right\rangle \left(n_i n_j - n_i^{eq} n_j^{eq} \right), \tag{47}$$

where the sum runs over all dark sector particles.

A more detailed look at the relic density calculation as-well as the relic density of The LKP is given in [30].

3.3 Constraints on DM

The most common solution to the dark matter problem is to attribute the extra matter density to some undiscovered particles which interact gravitationally and possibly weakly with other particle. Any such particle must be acompanied by an explaintion of why this particle is not yet detected by LHC searches or direct/indirect detection experiments. Indirect detection experiments look for possible products of DM-DM annihilation, primarily photon and neutrinos. As the expected flux should be proportional to the DM density squared we expect some otherwise unexplained particle production from places DM accumulate such as the galactic center. Direct detection looks for scattering events of atomic nuclei. Direct detection will be discussed in this section. A schematic description of direct detection, indirect detection and collider searches is given in in figure **??**

The DM particle is expected to be stable, non-relativistic, non-baryonic and dark. The particle has to be stable, or at least have a lifetime comparable to the age of the universe as it must still be present. Simulations of structure formation suggest that DM must be non-relativistic particles in order to explain the existence of large scale structures such as galaxies and clusters[18]. The Planck collaborations [2] found that less than 5% of the energy of the universe consists of baryonic matter, however dark matter makes up around 30% of the energy density, therefore most dark matter must be non-baryonic. Astronomicaly dark means it is electrically neutral, i.e. it does not interact with any kind of radiation as this would be detectable.

3.3.1 Direct detection

Direct detection experiments attempt to probe DM by looking for scattering events of atomic nuclei. If DM does indeed consist of WIMPs one would expect some non-zero, although usually small, cross section with nucleons and by extension atomic nuclei. Therefore a large sufficiently

isolated container filled with atomic nuclei will only interact with DM and will either detect the DM or place an upper bound on the nucleon-DM cross section. The best current bounds come from the XENON1T experiment which utilized a ton scale tank of liquid xenon [9] which gives an upper bound on the spin-independent DM-nucleon elastic cross section at 10^{-45}cm^2 for DM masses at TeV scales. The spin-dependent cross sections however the upper bound is at $2 \cdot 10^{-40}\text{cm}^2$ at the same DM mass scales [3]. For sufficiently heavy nuclei the spin-independent cross section is increased with a factor A^2 A being the mass number of the nucleus (number of protons+neutrons). This enhancement is due to the fact the even if the DM-nucleon cross section is small there are alot of nucleons to interact with. The cross sections for each nucleon add cohently hence thi efecti is called coherent enhancement [10]. For the spin dependent cross sections the no such enhancement happens as the spins are not aligned. This section is based on [16] and [48].

The event rate per unit detector mass is given by

$$\frac{dR}{d|\mathbf{q}|^2} = \frac{\rho}{m_N m_\chi} \int_{v_{min}}^{\infty} \frac{d\sigma}{d|\mathbf{q}|^2} v f(v) dv\,, \tag{48}$$

ρ being the DM massdensity, v is the relative velocity of the nucleon and DM particle, f(v) is the velocity distribution of DM relative to the detector, q^μ the transferred momentum which is related to the recoil energy of the nucleus by $E_r = |\mathbf{q}|^2/2m_N$. Meaning that 48 can be rewritten as

$$\frac{dR}{dE_r} = \frac{\rho}{m_\chi} \frac{d\sigma}{d|\mathbf{q}|^2} \int_{v_{min}}^{\infty} v f(v) dv\,. \tag{49}$$

The cross section gets contributions from both spin-dependent and spin-independent interactions

$$\frac{d\sigma}{d|\mathbf{q}|^2} = \left(\frac{d\sigma}{d|\mathbf{q}|^2}\right)_{SD} + \left(\frac{d\sigma}{d|\mathbf{q}|^2}\right)_{SI}\,. \tag{50}$$

The spin-(in)dependent cross section is given by

$$\left(\frac{d\sigma}{d|\mathbf{q}|^2}\right)_{SI/SD} = \frac{\sigma_0^{SI/SD}}{4\mu^2 v^2} F^2(|\mathbf{q}|^2)\,, \tag{51}$$

$\mu = \frac{m_\chi M}{m_\chi + M}$ being the reduced mass of the DM nucleus system and $F^2(|\mathbf{q}|)$ being the form factor which can be understood as the Fourier transform of the nuclear density distribution. The only particle physics input is the cross section evaluated at q=0 σ_0 which has to be understood by the the fundamental interactions between DM and quarks and gluons.

In order to calculate rates for different nuclei it is convenient to derive the effective four-point coupling constants for the nucleon-nucleon-DM-DM vertex In order to calculate these one must first compute every quark/gluon elastic scattering matrix element, splitting up the spin dependent and spin independent contributions. These matrix elements must be evaluated between the initial and final states, i.e. the nucleon state. Finally all these contributions are added together such that we have 4 effective couplings: one spin dependent and one spin independent for every nucleon.

The full nucleon-DM scattering process is then entirely captured by the following diagram:

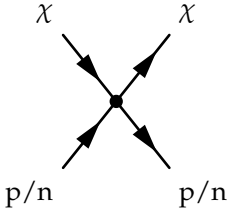

The spin-independent DM-nuclei cross sectoion will then be given by

$$\sigma_0^{SI} = \frac{1}{\pi}\left(\frac{M}{m_\chi + M}\right)^2 (Zf_p + (A-Z)f_n)^2 \,, \tag{52}$$

M being the nucleus mass, Z the atomic number and A the mass number, and f_N the nucleon couplings.

The spin-dependent cross section is given by

$$\sigma_0^{SD} = \frac{1}{\pi}\left(\frac{M}{m_\chi + M}\right)^2 \frac{8}{3}\frac{(J+1)}{J}\left(\langle S_p \rangle a_p + \langle S_n \rangle a_n\right)^2 \,, \tag{53}$$

$\langle S_N \rangle = \langle A | S_N | A \rangle$ being the expectation-value of total spin of the relevant nucleon in the nucleus, and J the spin of the nucleus. The next section will cover the calculation of the effective four-point coupling with the KK-photon in detail.

The full set of non-relativistic operators is given in [22]. The terms that depend on the velocities involved are subdominant, as the DM-velocities are small [34], and as such will not be considered here.

3.4 UED dark matter

The lightest KK-particle, the LKP, is one example of a WIMP, based on current collider bounds it has a mass larger than 1.4 TeV [11], which is in the appropriate range for a WIMP.

Conservation of KK-parity ensures that the LKP is stable as discussed in section 2.2. Ignoring radiative corrections it is clear that the KK-photon is the LKP, and in mUED this is still true after including radiatve corrections [23]. The KK-photon is a good DM-candidate as it is electrically neutral, non-baryonic, stable and non-relativistic. By virtue of being a typical WIMP it is expected to provide the appropriate relic density. When all co-annihilitions are included the theory gives the right relic density in the parameter region $R^{-1} = 1300 - 1500 GeV$ with $\Lambda R = 20$ [8] without finite corrections, for $\Lambda R = 50$ the upper bound is pushed up to 1600 GeV. When finite corrections are included the upper bounds are estimated to be 1660 GeV and 1785 GeV with $\Lambda R = 20$ and $\Lambda R = 50$ respectively [30].

Previous calculations of the KK-photon nucleon elastic cross sections [48] [28] [27], which were all done without finite corrections, have found that they are not excluded by direct detection experiments. Out of all these the largest spin independent proton-LKP cross section on the parameter region allowed by the relic density was given in [28] $3 \cdot 10^{-46}$ cm^2 around 1300 GeV, compared to the current bounds from direct detection experiments of 10^{-45} cm^2 these are all within the upper bound. The largest spin-dependent cross section at the same compactification scale was $4 \cdot 10^{-44}$ cm^2 while the upper bound is 10^{-40} cm^2. However the cross sections may change significantly when finite corrections are included. The cross sections including finite corrections will be presented in section 5.

4 Direct detection of the Kaluza-Klein photon

One of the goals of this thesis was to calculate the elastic scattering cross section for the first KK-mode of the photon with nucleons and atomic nuclei, in order to investigate whether it is a viable

candidate for DM based on current and projected direct detection bounds. This was done by implementing effective four-point couplings in the UED module in the DarkSUSY package [14]. DarkSUSY already contains routines for computing elastic scattering cross sections from the effective four-point couplings as well as providing all necessary couplings and masses.

This section presents the calculation of the effective four-point couplings. The first part is dedicated to setting up the calculation by giving the effective Lagrangian and relevant definitions and present the calculation of the quark and gluon contributions . The final part describes DarkSUSY and the newly direct detection part of the UED module.

4.1 Effective Lagrangian

We want to describe the elastic scattering of DM and nucleons as an effective theory involving only 3 particles, the DM-particle and the proton and neutron. As nucleons are composite particles consisting of quarks and gluons their interactions will at leading order be given by a sum over interactions with a single constituent weighted by the relative amount of said constituent in the nucleon. Therefore the first step is to express an effective theory, or equivalently write down a Lagrangian, of elastic scattering of DM with quarks and gluons.

As both the LKP and nucleus are non-relativistic particles any operators suppressed by he velocity of either particle can be neglected leaving the effective interaction Lagrangian derived by Hissano et al. [28]

$$\mathcal{L}_q^{\text{eff}} = f_q A^{(1)\mu} A_\mu^{(1)} (\bar{q} m_q q + \bar{q} i \not{D} q) + \frac{d_q}{m_{A^{(1)}}} \epsilon_{\mu\nu\rho\sigma} A^{(1)\mu} i\partial^\nu A^{(1)\rho} \bar{q} \gamma^\sigma \gamma^5 q + \frac{g_q}{m^2_{A^{(1)}}} i\partial^\mu A^{(1)\rho} i\partial^\nu A_\rho^{(1)} \mathcal{O}^q_{\mu\nu} , \tag{54}$$

The first term can be simplified by the Dirac equation $\bar{q} i \not{D} q = \bar{q} m_q q$ The second term here is spin-dependent as in 4D the helicity, the spin along the direction of motion of a particle, is the same as the chirality, the eigenvalue of γ^5. The gluon contribution can be model by the Lagrangian

$$\mathcal{L}_g^{\text{eff}} = f_g A^{(1)\mu} A_\mu^{(1)} G^a_{\mu\nu} G^{a\mu\nu} + \frac{g_G}{m^2_{A^{(1)}}} A^{(1)\rho} i\partial^\mu i\partial^\nu A_\rho^{(1)} \mathcal{O}^g_{\mu\nu} , \tag{55}$$

where $G^a_{\mu\nu}$ is the gluon field strength tensor and $\mathcal{O}^{g/q}_{\mu\nu}$ is the twist-2 operator defined as:

$$\mathcal{O}^q_{\mu\nu} = \frac{1}{2} i\bar{q} (D_\mu \gamma_\nu + D_\nu \gamma_\mu - \frac{1}{2} g_{\mu\nu} \not{D}) q , \tag{56}$$

$$\mathcal{O}^g_{\mu\nu} = G^{a\rho}_\mu G^a_{\rho\nu} + \frac{1}{4} g_{\mu\nu} G^{a\alpha\beta} G^a_{\alpha\beta} , \tag{57}$$

the twist of an operator is defined as mass dimension minus the spin.

Scattering amplitudes are given by the matrix element of the effective Lagrangian evaluated between the initial and final states. As the quarks and gluons that are of interest to direct detection are all in nucleon states as a constituent of a nucleon we only care about quark and gluon operators evaluated in nucleon states. Demoting the on-shell nucleon state as $|N\rangle$ ($N = n, p$).

$$\langle N | \bar{q} q | N \rangle = \frac{m_N}{m_q} f_{Tq} , \tag{58}$$

$$\langle N | G^a_{\mu\nu} G^{a\mu\nu} | N \rangle = -\frac{8\pi}{9\alpha_s} m_N f_{TG} , \tag{59}$$

where the quark contribution $f_{Tq/G}$ is calculated in [41] using lattice QCD, for $q = u, d$ these will not be the same for protons and neutrons. As the quark mass appears in the denominator we need to keep terms linear in m_q when computing the quark scattering diagrams.

Although the gluon-DM cross section do not receive any tree-level contribution the fact that the expression contains a factor $\frac{1}{\alpha_s}$ [**?**] means the contribution from 1-loop diagrams will be of the same order as the contribution from tree-level diagrams. This is not the case for the twist-2 which is loop-suppressed and will therefore be ignored.

The twist-2 operators evaluate to:

$$\langle N|\,\mathcal{O}^q_{\mu\nu}\,|N\rangle = \frac{1}{m_N}(p_\mu p_\nu - m_N^2\frac{1}{4}g_{\mu\nu})(q(2)+\bar{q}(2))\,, \tag{60}$$

$$\langle N|\,O^g_{\mu\nu}\,|N\rangle = \frac{1}{m_N}(p_\mu p_\nu - m_N^2\frac{1}{4}g_{\mu\nu})G(2)\,, \tag{61}$$

G(2), q(2) and $\bar{q}(2)$ being the second moment of the PDFs for gluons, quarks and anti-quarks respectively. Defined as

$$G(2) = \int_0^1 dx x f_g(x)\,, \tag{62}$$

$$q(2)+\bar{q}(2) = \int_0^1 dx x(f_q(x)+f_{\bar{q}}(x))\,, \tag{63}$$

which can be understood as the fraction x of of the total momentum of the nucleon carried by the relevant particle.

The spin-dependent term is evaluated as

$$\langle N|\,\bar{q}\gamma_\mu\gamma_5 q\,|N\rangle = 2s_\mu\Delta q_N\,, \tag{64}$$

s_μ being the spin of the nucleon and q_N being the spin contribution of the relevant quark obtained from [1]

Now we can finally express the spin-independet effective couplings f_N by using relating the scattering amplitude in the effective theory consisting of DM and nucleons and the effective theory with a single vertex to the same amplitude in the described by Eq. 54 and 55.

$$\mathcal{M}_{SI} = -i\epsilon_\mu(p^{in}_{\gamma^{(1)}})\epsilon^\mu(p^{out}_{\gamma^{(1)}})f_N = -i\,\langle N|\,\mathcal{L}_q^{SI\text{eff}} + \mathcal{L}_g^{SI\text{eff}}\,|N\rangle\,. \tag{65}$$

Preforming a Fourier transform, factoring out the polarization vectors ϵ and taking the non-relativistic limit $p^\mu_{\gamma^{(1)}}, p^\mu_N = (m_{\gamma^{(1)}}, \mathbf{0}), (m_N, \mathbf{0})$ we find

$$\frac{f_N}{m_N} = \sum_{q=u,d,s} f_q f_{T_q} + \sum_{q=u,d,s,c,b}\frac{3}{4}g_q(q(2)+\bar{q}(2)) - \frac{8\pi}{9\alpha_s}f_G f_{T_G}\,. \tag{66}$$

For the spin-dependent coupling we use the same argument

$$\mathcal{M}_{SD} = -i\epsilon_{\mu 0\rho\sigma}\epsilon^\mu(p^{in}_{\gamma^{(1)}})\epsilon^\rho(p^{out}_{\gamma^{(1)}})s^\sigma a_N = -i\,\langle N|\,\mathcal{L}_q^{SD\text{eff}}\,|N\rangle\,, \tag{67}$$

and find the effecitve coupling:

$$a_N = \sum_{q=u,d,s} d_q\Delta q_N\,. \tag{68}$$

The coefficients f_q, f_g, d_qandg_g are extracted from the scattering amplitudes of DM with quarks and gluons respectively as they are low energy effective couplings. This is done by computing the $q/g - DM \to q/g - DM$ matrix element in the limit where the no energy is exchanged.

4.1.1 Quark contribution

The following diagrams diagrams contribute to the quark-DM elastic scattering cross section:

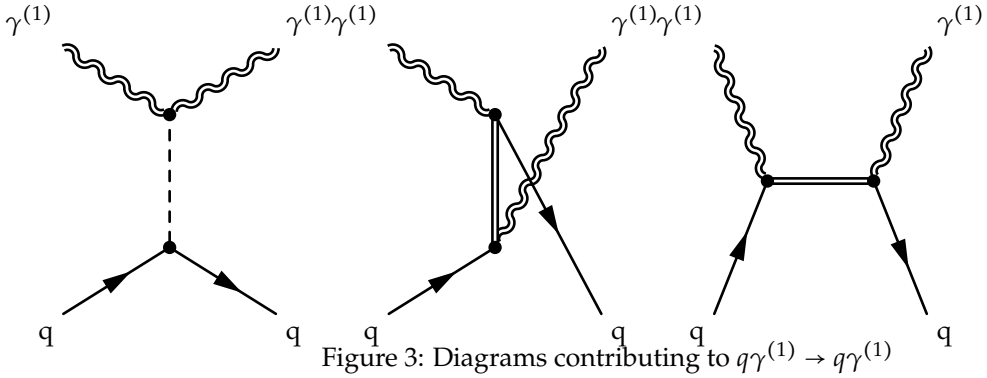

Figure 3: Diagrams contributing to $q\gamma^{(1)} \to q\gamma^{(1)}$

These diagrams have 4 external momenta, however as we are intersted in the $q^2 = 0$ limit, the limit where no energy is exchanged the incoming and outgoing DM momenta will be equal. As there are two external vectors the matrix element will be given by

$$\mathcal{M} = \epsilon_\mu(p^{in}_{\gamma^{(1)}})\epsilon^*_\nu(p^{out}_{\gamma^{(1)}})\mathcal{M}^{\mu\nu}\,, \tag{69}$$

ϵ_μ being the KK-photon polarization vector.

The Higgs exchange diagram evaluates to

$$\mathcal{M}^{\mu\nu}_h = ig_{\gamma^{(1)}\gamma^{(1)}h}\lambda_q\frac{g^{\mu\nu}}{m_h^2}\bar{q}q\,. \tag{70}$$

The exchanged KK-quarks can be either a singlet or a doublet. We also need to distinguish between the diagrams were the external quarks are right- and left-handed. This means each of the diagrams involving a KK-quark are actually 4 diagrams, although the DM-$q_R - q^{(1)}{}_d$ coupling and DM-$q_L - q^{(1)}{}_s$ coupling are suppressed. These diagrams are still included in the numerical implementation. It is worth noting that this suppression is not as strong for top-quarks, however the top-quark content in nucleons is so small that it has no impact here.

The KK-quark exchange diagrams evaluate to

$$\mathcal{M}^{\mu\nu}_{R/L} = -ig^2_{\gamma^{(1)}q^{(1)}{}_{s/d}q_{R/L}}\bar{q}_{R/L}\left(\gamma^\mu\frac{\not{p}_q - \not{p}_{\gamma^{(1)}} + m_{q^{(1)}_{s/d}}}{(p_q - p_{\gamma^{(1)}})^2 - m^2_{q^{(1)}_{s/d}}}\gamma^\nu + \gamma^\nu\frac{\not{p}_{\gamma^{(1)}} + \not{p}_q + m_{q^{(1)}_{s/d}}}{(p_{\gamma^{(1)}} + p_q)^2 - m^2_{q^{(1)}_{s/d}}}\gamma^\mu\right)q_{R/L}\,. \tag{71}$$

Focusing just on the numerator we have 4 distinct Dirac bi-linears

$$\bar{q}P_{L/R}\gamma^\mu\not{p}\gamma^\nu P_{R/L}q = \bar{q}\gamma^\mu\not{p}\gamma^\nu P_{R/L}P_{R/L}q = \bar{q}\gamma^\mu\not{p}\gamma^\nu P_{R/L}q\,,$$

$$\bar{q}P_{L/R}\gamma^\mu\gamma^\nu P_{R/L}q = \bar{q}\gamma^\mu\gamma^\nu P_{L/R}P_{R/L}q = 0\,,$$

the other two are related by exchange of indices. This leaves the following matrix element

$$\mathcal{M}^{\mu\nu}_{R/L} = -ig^2_{\gamma^{(1)}q^{(1)}q}\Big(\frac{p_{q\sigma}-p_{\gamma^{(1)}\sigma}}{(p_q-p_{\gamma^{(1)}})^2-m^2_{q^{(1)}}}\bar{q}\gamma^\mu\gamma^\sigma\gamma^\nu P_{R/L}q + \frac{p_{\gamma^{(1)}\sigma}+p_{q\sigma}}{(p_{\gamma^{(1)}}+p_q)^2-m^2_{q^{(1)}}}\bar{q}\gamma^\nu\gamma^\sigma\gamma^\mu P_{R/L}q\,. \quad (72)$$

This matrix element can conveniently be written as

$$\mathcal{M}^{\mu\nu}_{qR/L} = -ig^2_{\gamma^{(1)}q^{(1)}q}\big(c_\sigma(\bar{q}\gamma^\nu\gamma^\sigma\gamma^\mu+\gamma^\mu\gamma^\sigma\gamma^\nu q)+d_\sigma(\bar{q}\gamma^\nu\gamma^\sigma\gamma^\mu-\gamma^\mu\gamma^\sigma\gamma^\nu q)\big)\,. \quad (73)$$

This decomposition is convenient as the first term is spin independent and the second term contains all the spin-dependence as demonstrated shortly. The coefficients were found to be

$$c^\sigma = -\frac{(m^2_{\gamma^{(1)}}-{m_{q^{(1)}}}^2)p^\sigma_q + 2m_q m_{\gamma^{(1)}}p^\sigma_{\gamma^{(1)}}}{({m_{\gamma^{(1)}}}^2+2m_qm_{\gamma^{(1)}}-{m_{q^{(1)}}}^2)({m_{\gamma^{(1)}}}^2-2m_qm_{\gamma^{(1)}}-{m_{q^{(1)}}}^2)}\,, \quad (74)$$

$$d^\sigma = -\frac{(m^2_{\gamma^{(1)}}-m^2_{q^{(1)}})p^\sigma_{\gamma^{(1)}} + 2m_q m_{\gamma^{(1)}}p^\sigma_q}{({m_{\gamma^{(1)}}}^2-2m_qm_{\gamma^{(1)}}-m^2_{q^{(1)}})(m^2_{\gamma^{(1)}}+2m_qm_{\gamma^{(1)}}-m^2_{q^{(1)}})}\,. \quad (75)$$

When evaluating contraction of momenta the on-shell condition $p_\mu p^\mu = m^2$ and the contraction $p^\mu_g p_{kga\mu} = m_q m_{\gamma^{(1)}}$ was used. The second one can be justified as by the fact the KK-photon is non-relativistic.

Using basic Dirac algebra we can rewrite the bilinear in first term in 73 as

$$\bar{q}\gamma^\nu\gamma^\sigma\gamma^\mu q + (\mu\leftrightarrow\nu) = 2\bar{q}(g^{\mu\sigma}\gamma^\nu + g^{\nu\sigma}\gamma^\mu - g^{\mu\nu}\gamma^\sigma)q\,. \quad (76)$$

Looking at the index structure of c_σ we should look at the contraction:

$$p_{q\sigma}2\bar{q}(g^{\mu\sigma}\gamma^\nu + g^{\nu\sigma}\gamma^\mu - g^{\mu\nu}\gamma^\sigma)q = 2\bar{q}(p^\mu_q\gamma^\nu + p^\nu_q\gamma^\mu - g^{\mu\nu}\not{p}_q)q = 4\tilde{\mathcal{O}}^{q\mu\nu} - g^{\mu\nu}\bar{q}\not{p}_q q\,, \quad (77)$$

$$p_{\gamma^{(1)}\sigma}2\bar{q}(g^{\mu\sigma}\gamma^\nu + g^{\nu\sigma}\gamma^\mu - g^{\mu\nu}\gamma^\sigma)q = 2\bar{q}(p^\mu_{\gamma^{(1)}}\gamma^\nu + p^\nu_{\gamma^{(1)}}\gamma^\mu - g^{\mu\nu}\not{p}_{\gamma^{(1)}})q\,, \quad (78)$$

The terms proportional to $p^\mu_{\gamma^{(1)}}$ and $p^\nu_{\gamma^{(1)}}$ can be dropped as $\epsilon_\mu(p_{\gamma^{(1)}})p^\mu_{\gamma^{(1)}} = 0$. Taking the non-relativistic limit by fixing $p_{\gamma^{(1)}\mu} = (m_{\gamma^{(1)}},\mathbf{0})$ and using the fact that $\bar{q}\not{p}_q q = m_q\bar{q}q$ by the Dirac equation we get the scalar contribution to the spin independent martix element

$$\mathcal{M}^{\mu\nu}_{sq} = \mathcal{M}^{\mu\nu}_{sqR} + \mathcal{M}^{\mu\nu}_{sqR} + \mathcal{M}^{\mu\nu}_h = ig_{\gamma^{(1)}q^{(1)}q}{}^2\frac{({m_{\gamma^{(1)}}}^2-{m_{q^{(1)}}}^2)(4\mathcal{O}^{q\mu\nu}-m_qg^{\mu\nu}\bar{q}q)+m_q4{m_{\gamma^{(1)}}}^2g^{\mu\nu}\bar{q}q}{({m_{\gamma^{(1)}}}^2-2m_qm_{\gamma^{(1)}}-{m_{q^{(1)}}}^2)({m_{\gamma^{(1)}}}^2+2m_qm_{\gamma^{(1)}}-{m_{q^{(1)}}}^2)}$$
$$+ ig_{\gamma^{(1)}\gamma^{(1)}h}\lambda_q\frac{g^{\mu\nu}}{mh^2}\bar{q}q\,. \quad (79)$$

We have therefore determined 2 of the necessary coefficients from Eq. 54

$$g_q = -g^2_{\gamma^{(1)}q^{(1)}q}\frac{4(m^2_{\gamma^{(1)}} - m^2_{q^{(1)}})}{(m^2_{\gamma^{(1)}} - 2m_q m_{\gamma^{(1)}} - m^2_{q^{(1)}})(m^2_{\gamma^{(1)}} + 2m_q m_{\gamma^{(1)}} - m^2_{q^{(1)}})},$$

and

$$f_q = -g^2_{\gamma^{(1)}q^{(1)}q}\frac{(3m^2_{\gamma^{(1)}} + m^2_{q^{(1)}})}{(m^2_{\gamma^{(1)}} + 2m_q m_{\gamma^{(1)}} - m^2_{q^{(1)}})(m^2_{\gamma^{(1)}} + 2m_q m_{\gamma^{(1)}} - m^2_{q^{(1)}})} + \frac{\lambda_q g_{\gamma^{(1)}\gamma^{(1)}h}}{m_q m_h^2}.$$

For the second term in Eq. 73 we use the Chisholm identity to write the spin dependent matrix element as:

$$\mathcal{M}^{\mu\nu}_{spin} = d_\sigma \bar{q}\gamma^\nu\gamma^\sigma\gamma^\mu - \gamma^\mu\gamma^\sigma\gamma^\nu q = d_\sigma \bar{q} 2i\epsilon^{\mu\nu\sigma\rho}\gamma^5\gamma_\rho q\,,$$

which allows us to recognize the coefficient d_q in the nonrelativistic limit:

$$d_q = -ig^2_{\gamma^{(1)}q^{(1)}q}\frac{m_{\gamma^{(1)}}(m^2_{\gamma^{(1)}} - m^2_{q^{(1)}})}{4(m^2_{\gamma^{(1)}} + 2m_q m_{\gamma^{(1)}} - m^2_{q^{(1)}})(m^2_{\gamma^{(1)}} + 2m_q m_{\gamma^{(1)}} - m^2_{q^{(1)}})}.$$

4.1.2 Gluon contribution

The gluon-DM elastic scattering process gets contribution from the following diagrams:

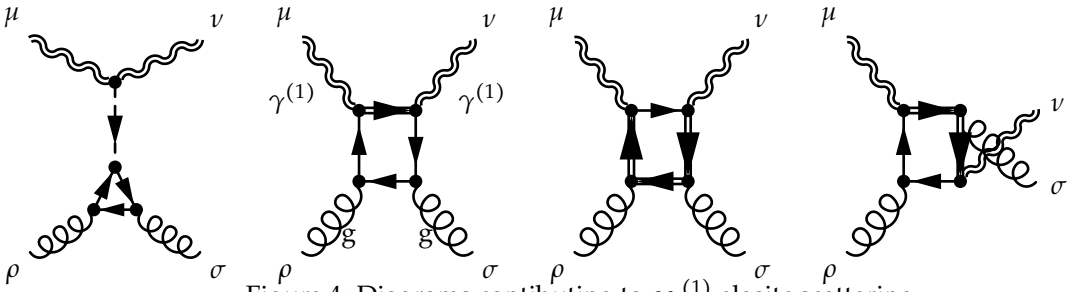

Figure 4: Diagrams contibuting to $g\gamma^{(1)}$ elasitc scattering

The first diagram is suppressed due to the Yukawa coupling which is proportional to m_q . Unlike the quark contribution there is no cancellation of this quark mass.

The amplitude is given by

$$\mathcal{M} = \epsilon_\mu(p_{\gamma^{(1)}})\epsilon_\nu(p_{\gamma^{(1)}})\epsilon_\rho(p_g)\epsilon_\sigma(p_g)\mathcal{M}^{\mu\nu\rho\sigma}\,. \tag{80}$$

The fermion loops give rise traces over gamma matrices from vertices and fermion propagators. The two gluon vertices in each diagram only contain a vector coupling and only contributes one gamma matrix. On the other hand the (KK-photon)-(KK-quark)-(SM-quark) vertices does not treat right handed and left handed quarks equally and thus contributes $\gamma^\lambda P_{R/L}$ with distinct couplings. It is convenient to reformulate the left- and right-handed couplings as a vector coupling and an axial-vector coupling. This specific vertex, which can be obtained from the Feynmann rules given in [13], can be rewritten as:

$$g_{\gamma^{(1)}q^{(1)}{}_d q}\gamma^\lambda = (T_3 g\cos\alpha^1 s_w + Y_d g_y \cos\alpha^1 c_w)\gamma^\lambda \tfrac{1}{2}(1-\gamma^5) + c_w Y_s g_y \sin\alpha\gamma^\lambda \tfrac{1}{2}(1+\gamma^5)$$
$$= (T_3 g\cos\alpha^1 s_w + Y_d g_y \cos\alpha^1 c_w + c_w Y_s g_y \sin\alpha\tfrac{1}{2})\gamma c_w^\lambda + (-T_3 g\cos\alpha^1 s_w - Y_d g_y \cos\alpha^1 c_w Y_s g_y \sin\alpha)\gamma^\lambda\gamma^5$$
$$= g_v\gamma^\lambda + g_a\gamma^\lambda\gamma^5\,. \quad (81)$$

The shorthand $s_w = \sin\left(\theta^{(1)}\right)$, $c_w = \cos\left(\theta^{(1)}\right)$ is used here. The vertex rule for a the singlet KK-quark, KK-photon, SM-quark vertex is obtained by exchanging $\sin\left(\alpha^1\right)$ and $\cos\left(\alpha^1\right)$, and changing the overall sign.

The full trace over the whole fermion loop can then be split in two, one trace containing no γ^5s, the vector contribution, and one containing 2, the axial vector contribution. Any trace involving one γ^5 will evaluate to 0.

Let us look at just the contribution to the over all trace starting with the gamma matrecies introduced by the vertex involving the initial KK-photon γ^μ ($\gamma^\mu\gamma^5$) and the vertex involving the final KK-photon γ^ν ($\gamma^\nu\gamma^5$). Ignoring SM quark masses the first 2 box-diagrams give a vector contribution $\mathrm{Tr}\left(...\gamma^\mu \not{q}\gamma^\nu...\right)$ and an axial-vector contribution

$$\mathrm{Tr}\left(...\gamma^\mu\gamma^5\not{q}\gamma^\nu\gamma^5...\right) = \mathrm{Tr}\left(...\gamma^\mu\gamma^5\gamma^5\not{q}\gamma^\nu...\right) = \mathrm{Tr}\left(...\gamma^\mu\not{q}\gamma^\nu...\right). \quad (82)$$

While the propagator between the relevant couplings in the first case is $\not{q} + m_{q^{(1)}}$ the trace involving the mass term contains 7 gamma matrices and as such evaluate to 0. Thus the vector contribution and axial-vector contribution from the first 2 box diagrams are equal.

For the last box diagram a similar argument shows that the axial-vector contribution is related to the vector contribution by the replacement $m^2_{q^{(1)}} \to -m^2_{q^{(1)}}$

This distinction allows the matrix element to be written as

$$\mathcal{M}^{\mu\nu\sigma\rho} = -i\alpha_s\frac{2}{9}(g_v^2\mathcal{M}_v^{\mu\nu\sigma\rho} + g_a^2\mathcal{M}_a^{\mu\nu\sigma\rho})\,, \quad (83)$$

where $\mathcal{M}_v^{\mu\nu\sigma\rho}$ ($\mathcal{M}_a^{\mu\nu\sigma\rho}$) contains the (axial-)vector contribution. The factor $\frac{2}{9}$ is a group theory factor arising from the fact the gluon vertecies involve an SU(3)-generator [53].

Both the KK-photon and gluon polarization vectors satisfy the condition $\epsilon_\mu(p_g)p_g^\mu = \epsilon_\mu(p_{\gamma^{(1)}})p^\mu_{\gamma^{(1)}} =$ 0.In addition the gluons being mass less are also transverse in space $\epsilon_i(p_g)p_g^i = 0$. Combining the two conditions for gluon polarization vectors $\epsilon_\mu(p_g)p_g^\mu = \epsilon_0(p_g)p_g^0 + \epsilon_i(p_g)p_g^i = \epsilon_0(p_g)p_g^0 = 0$ we see that $\epsilon_0(p_g) = 0$. In the non-relativistic limit $p_{\gamma^{(1)}} = (m_{\gamma^{(1)}}, \mathbf{0})$ we therefore have an the condition: $\epsilon_\mu(p_g)p^\mu_{\gamma^{(1)}} = 0$. This means any term with an index carried by a KK-photon momentum will not contribute to the scattering amplitude. This means we can decompose the Lorentz-structure of the polarization tensor as:

$$\mathcal{M}^{\mu\nu\sigma\rho}_{v/a} = -\frac{B_{6v/a}}{m^2_{\gamma^{(1)}}}p_g^\mu p_g^\nu g^{\sigma\rho} + C_{1v/a}g^{\mu\nu}g^{\sigma\rho} + C_{2v/a}g^{\mu\sigma}g^{\nu\rho} + C_{3v/a}g^{\mu\rho}g^{\nu\sigma}\,, \quad (84)$$

where $C_{1v/a} = -\frac{1}{2}B_{1v/a}$, $C_{3v/a} = C_{2v/a} = B_{2v/a}$.

The coefficients B_6 , $B_{2v/a}$ and $B_{1v/a}$ are calculated in appendix A using the Passarino-Veltmann [42] Reduction scheme by making slight modifications to the program used in [37]. This program used Lerg [50] for calculating the annihilation cross section of two KK-hypercharge bosons to

photons which uses box diagrams related to the ones used here by crossing-symmetry. The minus sign is due to exchanging an outgoing momentum for an incoming one, so that all momenta can be considered as incoming when computing the diagrams.

Combining Eq. 83 and 84 the full matrix element for gluon-DM scattering is given by summing the vector and axial vector contributions:

$$\mathcal{M}^{\mu\nu\sigma\rho} = -i\alpha_s \frac{2}{9}(g_v^2)(-\frac{B_{6v}}{m^2_{\gamma^{(1)}}} p_g^\mu p_g^\nu g^{\sigma\rho} + C_{1v} g^{\mu\nu} g^{\sigma\rho} + C_{2v} g^{\mu\sigma} g^{\nu\rho} + C_{3v} g^{\mu\rho} g^{\nu\sigma}) + (v \to a)\,. \tag{85}$$

We now have to identify the Fourier transform of the term

$$G^a_{\rho\sigma} G^{a\rho\sigma} = (\partial_{[\rho} G^a_{\sigma]} - g_s f^{abc} G^b_\rho G^c_\sigma)^2\,, \tag{86}$$

making use of the identities $\epsilon_\mu(p_g) p_g^\mu = 0$ and $p_g^\mu p_{g\mu} = 0$ we find that:

$$\mathcal{M}^{\mu\nu\sigma\rho} = -i\alpha_s g_v^2 (-\frac{B_6}{m^2_{\gamma^{(1)}}} \tilde{\mathcal{O}}^{g\mu\nu} g^{\rho\sigma} + (C_{1v} - \frac{B_{6v} m_N^2}{4 m^2_{\gamma^{(1)}}}) g^{\mu\nu} g^{\rho\sigma}) + (v \to a)\,. \tag{87}$$

Comparing this expression to the effective Lagrangian 55 we can the read of the relevant effective coupling:

$$f_g m^2_{\gamma^{(1)}} = \alpha_s (g_v^2 (C_{1v} - \frac{B_{6v} m_N^2}{4 m^2_{\gamma^{(1)}}}) + g_a^2 (C_{1a} - \frac{B_{6a} m_N^2}{4 m^2_{\gamma^{(1)}}}))\,. \tag{88}$$

4.2 DarkSUSY

DarkSUSY [14] is FORTRAN package used for numerical calculations of among other things direct and indirect detection rates and relic densities for several different dark matter candidates. DarkSUSY consist of a core library which contains all model independent routines and particle modules which contain the model-specific routines. As of writing this thesis DarkSUSY contains a module for the minimal supersymmetric standard model, the Silveria-Zee model, a generic WIMP model, a generic model for decaying dark matter, a dark sector model with velocity dependent self-interactions and the as of yet unpublished UED module. An important part of this thesis has been implementing the direct detection routines in the UED module.

In order to calculate something using DarkSUSY the user has to supply a main program that specifies model parameters, in the case of mUED these are R^{-1}andΛ, and set up the relevant particle module. When the module is set up the user can make use of several routines in the core library which returns the desired observable(s), for direct detection these could for example be the scattering cross section with some nucleus or the recoil-rates for a specified experimental setup. The only model-specific input needed by the direct detection routines in the core library are the effective four-point couplings which are supplied by the routine dsddgpgn in the relevant particle module. As such the effective couplings derived in the previous section were implemented making use of the fact that all relevant masses and couplings, including radiative corrections were already part of the UED module [30].

4.2.1 The direct detection routines

The direct detection part of the UED module currently contains 6 subroutines/functions. The subroutine dsddgpgn returns the effective four-point couplings and makes calls to the others. The subroutines/functions dsdd_qsi, dsdd_twist2, dsdd_gluon and dsdd_sd takes as an input one SM-quark and one KK-quark and returns the relevant parameters f_q^h, f_q^q, g_q, f_g and d_q for the specified quark and KK-quark. In order to calculate the full effective fourpoint couplings dsddgpgn implements Eq. 66 by looping over all the quarks which are summed over by, note that the gluon contribuntion requires a sum over all quarks flavours. This includes one call for the singlet and one for the doublet KK-quark. The subroutine dsddboxcoeffs is only called within dsdd_gloun and takes the KK-quark as input and returns the Passarino-Veltmann coefficents cacluated in Appendix A.

5 Results

The effective four point coupling $\frac{f_p}{m_{\gamma^{(1)}}}$ is given by 66.

The scalar quark contribution f_q to the spin-independent effective coupling gets contributions from the Higgs exchange diagram and the KK-quark exchange diagrams labeled with a superscript. The Higgs exchange contribution is:

$$f_q^h = -\frac{m_W}{g}(g_Y \cos\left(\theta^{(1)}\right) - g \sin\left(\theta^{(1)}\right))^2 \frac{\lambda_q}{m_q m_h^2} \tag{89}$$

The KK-photon, KK-photon, SM-higgs vertex which has been explicitly included here is given in [30]. The only UED parameter that enters here is the weak mixing angle $\theta_w^{(1)}$ defined in 41. For the mass corrections we have $\delta m^{(n)} \propto \frac{n}{R}$ [23] meaning that the mixing angle for higher excitation will be small. I fact within the allowed parameter space $\sin^2(\theta_w^{(1)}) < 10^{-3}$, hence this contribution is only weakly dependant on the compactification scale.

The KK-quark exchange contribution is:

$$f_q^q = -g^2_{\gamma^{(1)}qq^{(1)}} \frac{3m^2_{\gamma^{(1)}} + m^2_{q^{(1)}}}{(m^2_{\gamma^{(1)}} - m^2_{q^{(1)}})^2} \tag{90}$$

Where the coupling $g_{\gamma^{(1)}qq^{(1)}}$ defined in 4.1.2 is kept implicit in the interest of keeping the expression compact.

The spin independent quark-DM effective coupling also get a a quark-twist-2 contribution:

$$g_q = -g^2_{\gamma^{(1)}qq^{(1)}} \frac{4}{(m^2_{\gamma^{(1)}} - m^2_{q^{(1)}})} \tag{91}$$

The gluon contribution to the spin independent cross section was found to be:

$$f_g = (g_v^2 C_{1v} + g_a^2 C_{1a} + (g_v^2 + g_a^2)\frac{B_6 m_n^2}{m^2_{\gamma^{(1)}}})\frac{\alpha_s}{9(4\pi)m^2_{\gamma^{(1)}}} \tag{92}$$

where C_{1v}, C_{1a} and B_6 are Passarino-Veltmann coefficients explicitly given in Appendix A, the evaluation of these loop-diagrams does indeed constitute one of the main results of this thesis.

The spin dependent proton-LKP cross section are given by:

$$\sigma_{SD} = \frac{\mu^2}{\pi} \sum_{s,d} \sum_{q=u,d,s} \left(\frac{g_{\gamma^{(1)} q^{(1)}_q} \Delta q_p}{4(m^2_{\gamma^{(1)}} - m^2_{q^{(1)}_{s/d}})} \right)^2 \tag{93}$$

where the first sum runs over singlet and doublet KK-quark.

5.1 Comparison with earlier results

The effective 4-point couplings and proton-DM elastic cross sections have previously been calculated by Hisano et al. [28], as this is an independent calculation to the ones preformed here it provides an important crosscheck of the numerical implementation. They calculated the cross sections using the radiative corrections from Cheng et al. [17], approximated the LKP by the hypercharge boson $B^{(1)}_\mu$ and for the spin dependent cross section assumed SM masses were negligible and all KK-masses except the LKP were degenerate using the splitting between the LKP and the other KK-particles as a free parameter. These results gave a good correspondence as shown in figure 5 and 6 which shows a comparison between [28] and the results obtained in this thesis as implemented in DarkSUSY in this limit.

The $B^{(1)} - B^{(1)} - H^{(0)}$ vertex factors used by Hissano et. al. differ from the one used in DarkSUSY by a factor of 2. The DarkSUSY coupling does however agrees with other sources [48], [13]. In figure 5 the vertex has for the purpose of comparison been set to the value given by Hissano et. al. [28].

The XENON1T bounds [9] are indicated in figure 5. As XENON1T has not registered any signal we know that the DM-proton cross section must be too small to be detected, hence the sensitivity of the experiment gives us an upper bound.

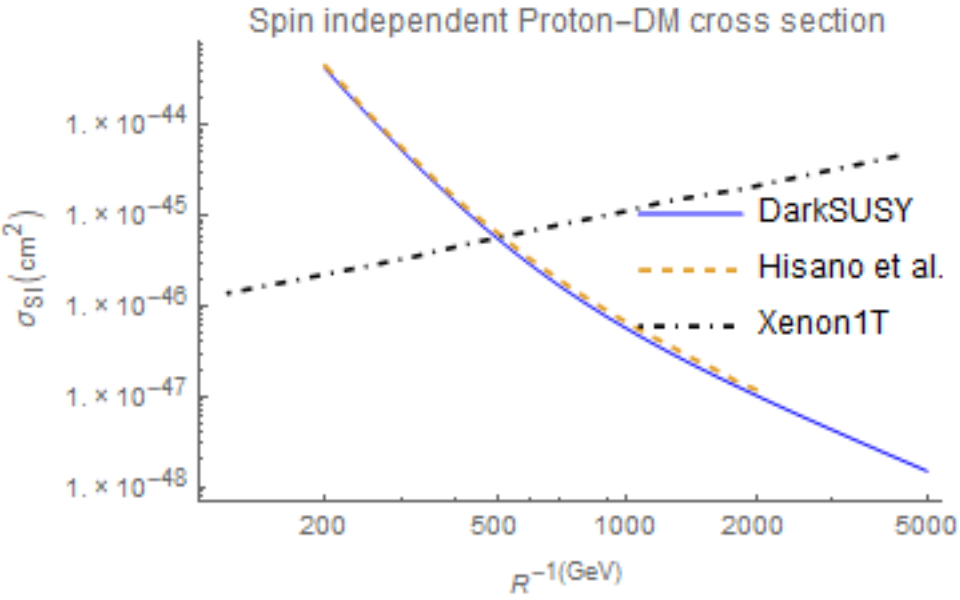

Figure 5: Comparison of the spin-independent cross section obtained in this thesis as implimented in DarkSUSY and Hissano et al [28] The 90% confidence bound from the Xenon1T experiment [9] is also shown

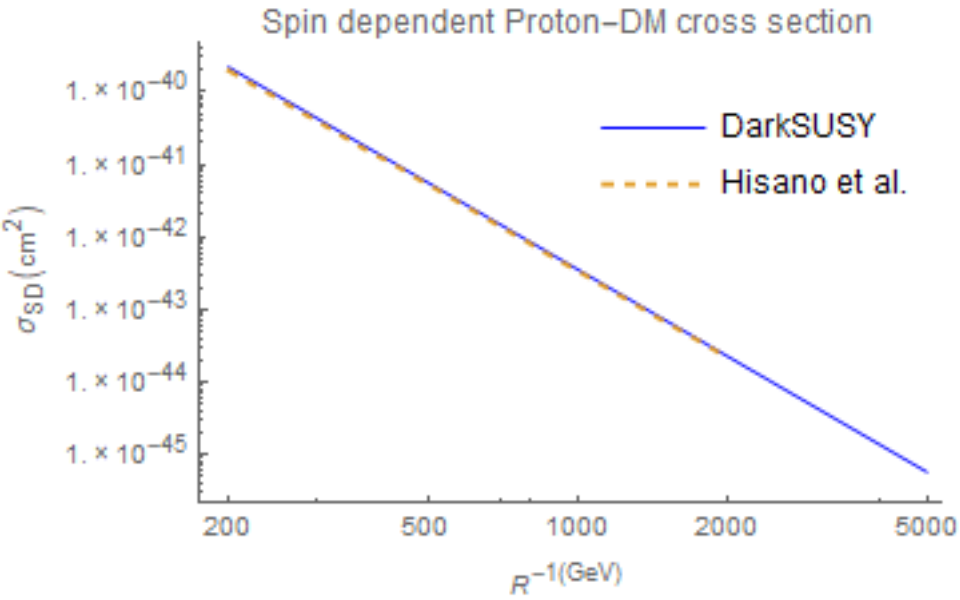

Figure 6: Comparison of the spin-dependent cross section obtained in this thesis as implimented in DarkSUSY and Hissano et al [28]

5.2 mUED cross sections

In figure 7 the spin-independent cross sections calculated in mUED using the full radiative correction are shown for different choices of Λ. Choosing a larger cutoff relaxes the mass degeneracy through radiative correction thereby reducing the cross section as all contributions except f_q^h defined in Eq. 89 are inversely proportional to the mass splitting $\Delta_q = \frac{m_{q^{(1)}} - m_{\gamma^{(1)}}}{m_{\gamma^{(1)}}}$. For larger R^{-1} the choice of Λ is less important as f_q^h dominates this regime. To show this behavior explicitly figure 8 shows each contribution to f_p where $\Lambda = 20R^{-1}$.

The spin-independent and spin-dependent cross section are given in figure 7 and 9 respectively. In both the spin independent and spin-dependent case a larger cutoff decreases the cross section by relaxing the degeneracy. However this effect is fairly consistent across all values of R^{-1} with the ratio $\frac{\sigma_{\Lambda=50}}{\sigma_{\Lambda=20}}$ ranging from 0.69 to 0.63 when R^{-1} is varied from 200 to 2000 GeV.

At the lower bound on R^{-1} = 1400GeV from LHC searches [11] the spin independent cross section takes values $4.1 \cdot 10^{-47}$ and $4.0 \cdot 10^{-47}\text{cm}^2$ for $\Lambda = \frac{20}{R}$ and $\Lambda = \frac{50}{R}$ respectively. The spin-dependent cross sections at this bound was found to be $6.3 \cdot 10^{-44}$ and $4.0 \cdot 10^{-44}\text{cm}^2$.

For larger R^{-1} we find a significantly smaller spin-independent cross section than Hissano et. al. [28]. Their cross sections do not include finite corrections and approximate the LKP by the KK-hypercharge boson $B^{(1)}$. Based on the effect introducing finite corrections have on the cross sections, which will be discussed shortly, and the fact the mixing angle Eq. 41 should be small for large R^{-1} we should expect better agreement for R^{-1} . The opposite seems to be the case here. For large R^{-1} we expect this to be explained by the Higgs contribution alone. This discrepancy is likely due to the $B^{(1)} - B^{(1)} - H^{(0)}$ vertex factors as discussed in the previous section.

The spin-dependant cross sections obtained here are slightly smaller than Hissano et. al. This difference is actually smaller than the difference than the difference between spin-dependent cross section with and without finite corrections found here, as presented in the next section. For small R^{-1} the difference is likely due to the fact they used $B^{(1)}$ as the LKP whereas the results obtained here used the KK-photon. The reduction in the cross section due to finite corrections is somewhat offset by the fact $\Lambda R = 20$ does not exactly correspond to $\Delta_q = 0.2$.

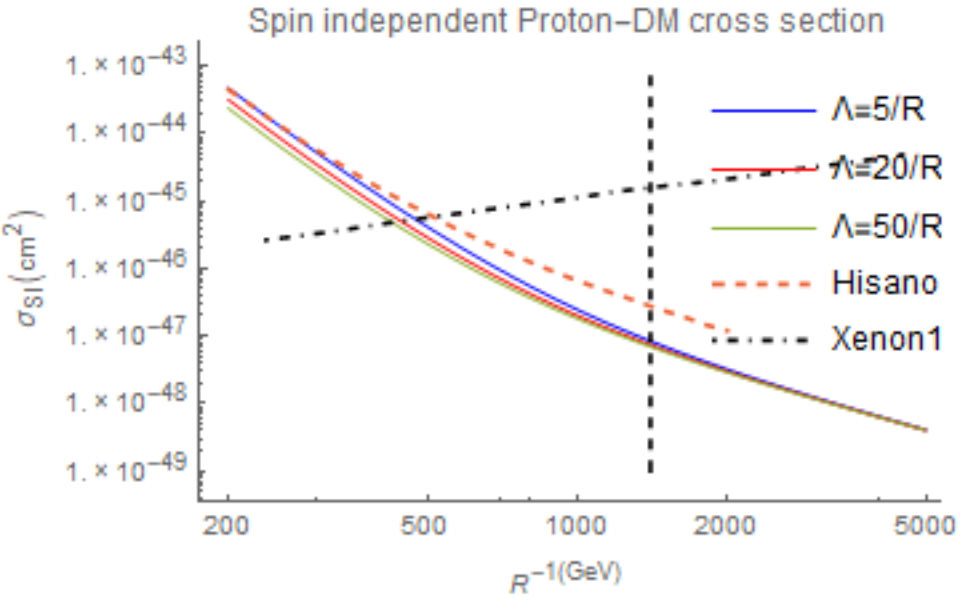

Figure 7: Spin-independent cross sections for $\Lambda R = 5, 20, 50$ obtain in this thesis as implemented in DarkSUSY compared to the results obtained by Hissano [28] with $\Lambda R = 20$ and the Xenon1T bound [9]. The vertical dashed black line indicates the LHC bound [11]

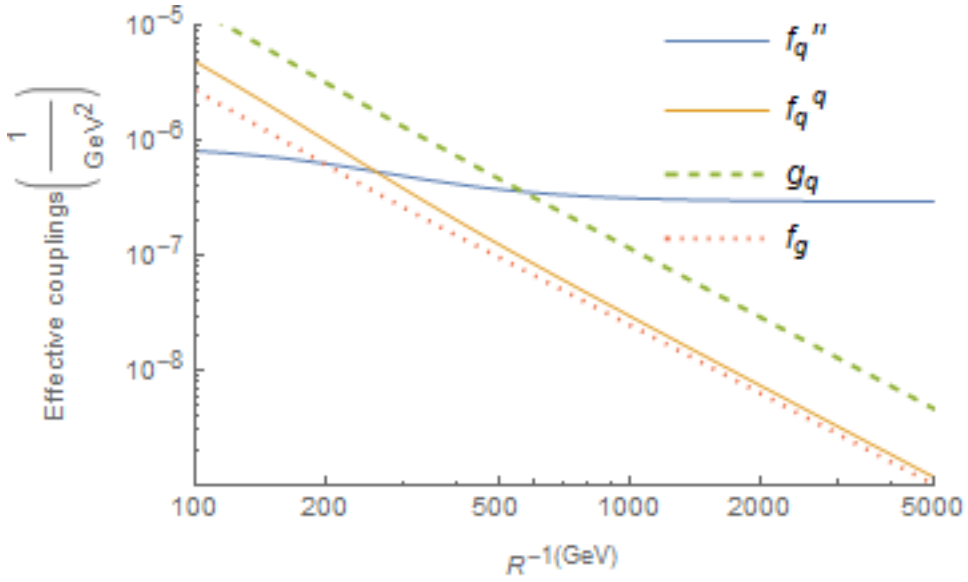

Figure 8: Contributions to the effective coupling $\frac{f_p}{m_{\gamma^{(1)}}}$ defined in 66 at $\Lambda R = 20$. The different contributions correspond to the exchange of a single SM Higgs boson (f_q^h)89, the scalar quark contribution (f_q^q) 90, the quark twist-2 contribution (g_q) 91 and the gluon contribution (f_g)92 respectively

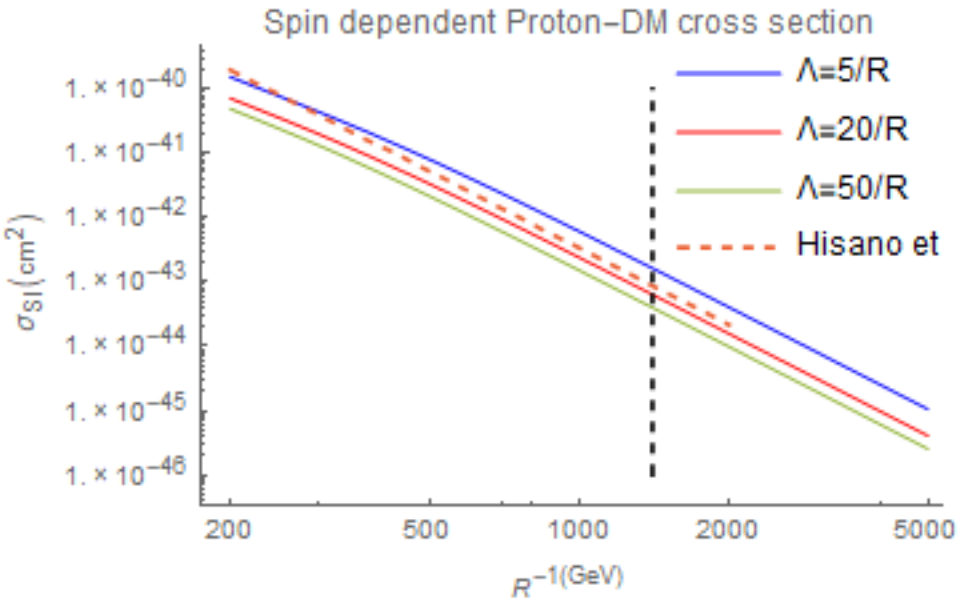

Figure 9: Spin-dependent cross sections for $\Lambda R = 5, 20, 50$ obtain in this thesis as implemented in DarkSUSY compared to the results obtained by Hissano [28] with $\Delta_q = \frac{m_{q^{(1)}} - m_{\gamma^{(1)}}}{m_{\gamma^{(1)}}} = 0.2$ witch approximatly corresponds to $\Lambda R = 20$. The vertical dashed black line inicates the LHC bound [11]

5.3 nonminimal effects

Figure 10 shows the spin independent cross sections of the KK-photon with the proton. Here the mass splitting $\Delta_q = \frac{m_{q^{(1)}} - m_{\gamma^{(1)}}}{m_{\gamma^{(1)}}}$ has been varied from 0.01 to 0.5 for all quarks excluding the top-quarks simultaneously. The cross section is enhanced as the KK-quarks and the KK-photon become degenerate.

As the degeneracy is lifted, i.e Δ_q is increased, the cross sections saturate as f_q^h does not depend on Δ_q whereas the other contributions decrease. Therefore when Δ_q is sufficiently large f_q^h is the only relevant contribution. This saturation happens faster for larger R^{-1} as f_q^h is more dominant in this regime, for $R^{-1} > \mathcal{O}(TeV)$ this happens before the mUED values of 0.2-0.25.

The spin-dependent cross sections are shown in figure 11 we again see that increasing the mass splitting decreases the cross sections for the same reasons as in the spin-independent case. However the spin-dependant cross sections have a consistent behavior as the compactification scale changes and do not saturate.

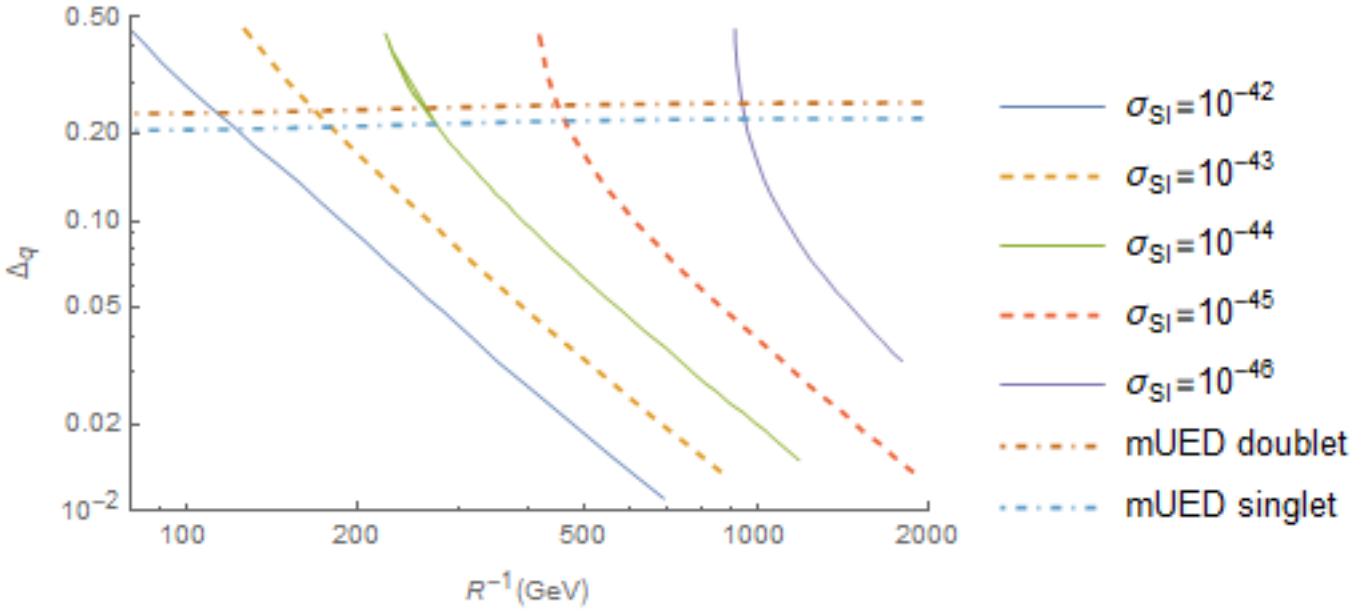

Figure 10: Spin-independent cross section with a proton in the degeneracy $\Delta_q = \frac{m_{q^{(1)}} - m_{\gamma^{(1)}}}{m_{\gamma^{(1)}}}$, R^{-1} plane where the degeneracy was fixed for all quarks except the top-quark which were kept at the mUED value which are shown as dotted lines for reference

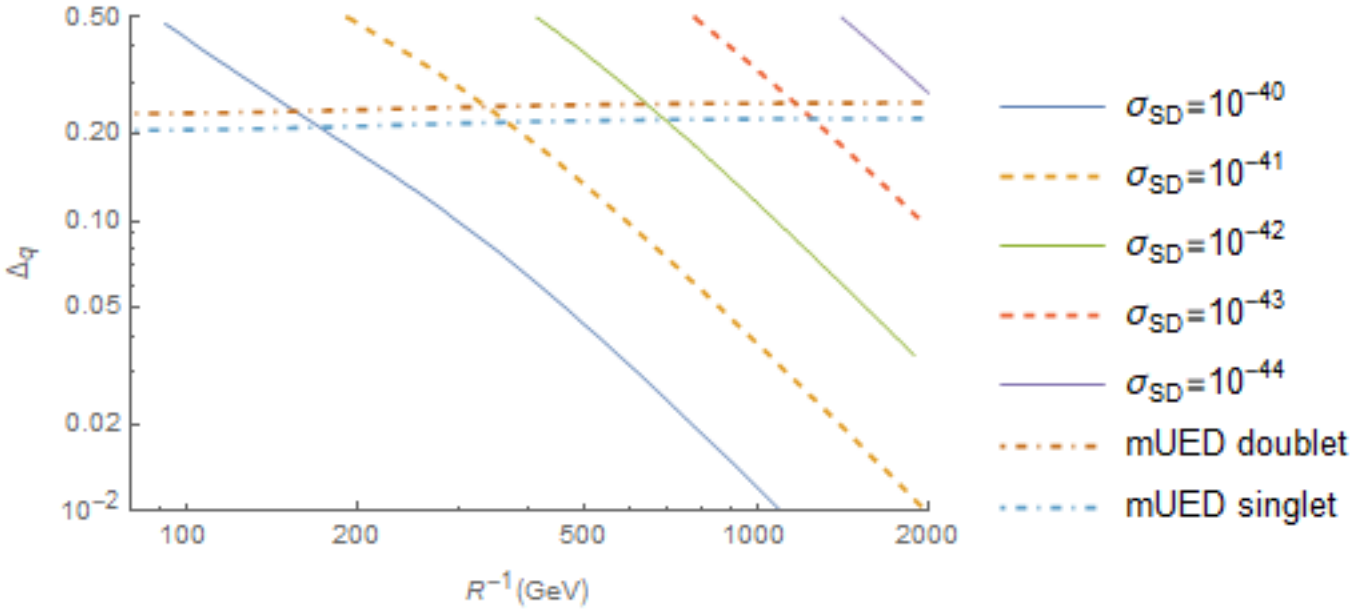

Figure 11: Spin-dependent cross section with a proton in the degeneracy $\Delta_q = \frac{m_{q^{(1)}} - m_{\gamma^{(1)}}}{m_{\gamma^{(1)}}}$, R^{-1} plhane were the degeneracy was fixed for all quarks except the top-quark which were kept at the mUED value which are shown as dotted lines for reference

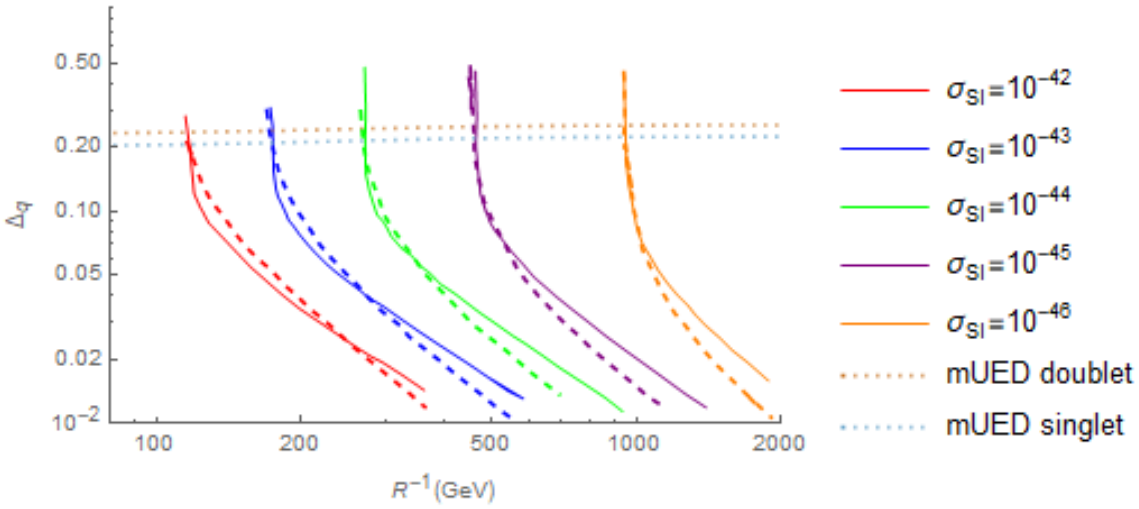

Figure 12: Spin-independent cross section with a proton in the degeneracy $\Delta_q = \frac{m_{q(1)} - m_{\gamma(1)}}{m_{\gamma(1)}}$, R^{-1} plane were the degeneracy was fixed for the down-quark(filled lines) or up-quark(dashed lines) while all others kept mUED values which are shown as dotted lines for reference

When we instead fix the mass of one KK-quark figure 12, keeping all others at the mUED value, we again find the cross sections are enhanced for values of small values of Δ_q, the enhancement is not as strong as in figure 10. For values of Δ_q above 0.1 the cross sections again become independent of Δ_q, however the cross sections tend towards larger values than in figure 10, as the contribution from the exchange of the KK-quarks whose masses are not varied are still significant. The difference however is smaller for larger R^{-1} with the 10^{-46}cm^2 contours being almost identical for Δ_q larger than the mUED value regardless of whether we fixed the mass one or all KK-quarks.

For values of $\Delta_{u/d/s/c/b} > 0.1$, the choice of which quark mass to vary made no appreciable difference, as the dominant contribution in this regime f_q^h is identical for all quarks, recall that $m_q = \frac{\lambda_q v}{\sqrt{2}}$.

For values smaller than 0.1 we see that the contours are slightly steeper for the up-quarks than the down-quarks. In this regime the scalar quark contribution (f_q^q) 90, the twist-2 contribution (g_q) 91 and the gluon contribution (f_g) 92 arising from the exchange of (or loop containing) the relevant KK-quark is expected to dominate.

The only difference between the up-quark and down-quark contribution in this regime is the vertex $g_{\gamma^{(1)}q^{(1)}{}_{s/d}q}$, for doublet KK-quarks this factor is almost identical for up-quarks and down-quarks, for singlet quarks however the vertex involving an up quark is larger than the one involving a down-quark by almost a factor of 2. Therefore the cross sections increase slightly faster when Δ_u is increases than when compared to the case when Δ_d is increased as the term that becomes dominant is larger.

5.4 Effect of finite corrections

Here we compare the cross sections calculated using only mass correction proportional to $\ln\left(\frac{\Lambda}{R^{-1}}\right)$ which were calculated in [17] and the cross sections calculated using mass correction from [23] which include finite corrections. As the finite corrections were calculated recently, this is the first time the direct detection cross section have been calculated. Figures 13 and 14 show the spin-independent and spin-dependent cross sections respectively with and without finite corrections with $\Lambda = \frac{20}{R}$.

The most important impact of finite corrections is that they increase the mass of KK-quarks and thus the mass splitting of the KK-quarks and KK-photons.

Both spin-dependent and spin-independent cross section are reduced when the finite corrections are added. The spin-dependent cross sections by a fairly constant overall factor

For the spin-independent cross section finite corrections are less important for large R^{-1} , as f_q^h which does not depend on the KK-masses, dominates in this region.

In order to make this clearer figure 15 shows the ratio between the cross sections calculated using only logarithmic contributions to the radiative correction as calculated by [17](σ_{old}) and the cross section including the finite corrections from (σ_{new}) [23].

Including the radiative correction reduces the spin dependent cross sections by up to 40 % . In the spin-dependant case the finite contributions cause a 20% decrease around R^{-1} = 1 TeV, but are less important for as R^{-1} is increased to the point where the finite correction do not make a difference above 3 TeV.

In general the finite corrections are more important for smaller cutoffs as the mass correction as the logarithmic term proportional to $\ln(\Lambda R)$ which the new and old corrections have in common will obviously be smaller. Therefore adding the same finite contribution will therefore not have as large of an impact on the cross sections.

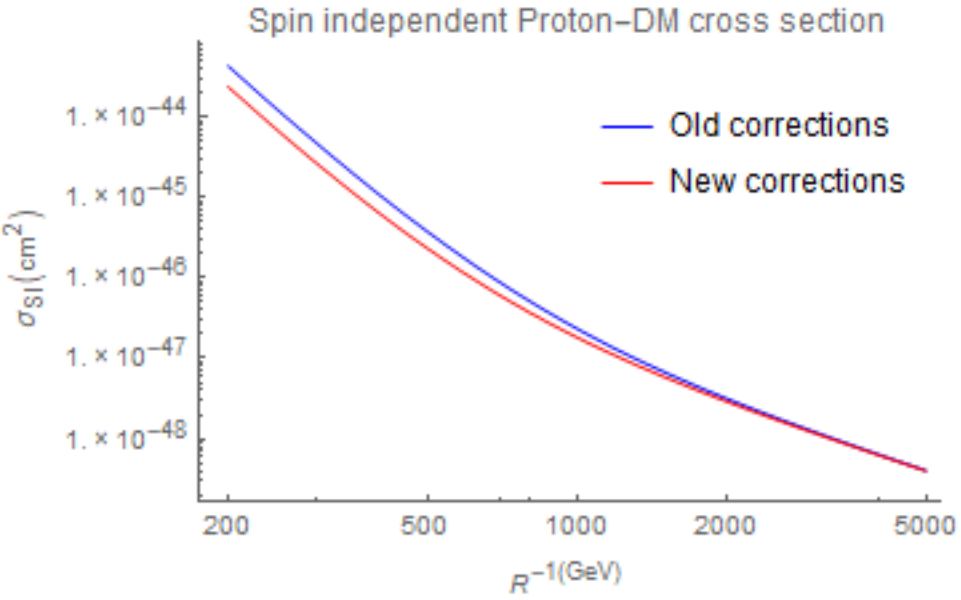

Figure 13: Comparision of the spin-independent cross sections calculated using radiative correction from [17] (Old corrections) and [23] (New Corrections) respectively and $\Lambda R = 20$

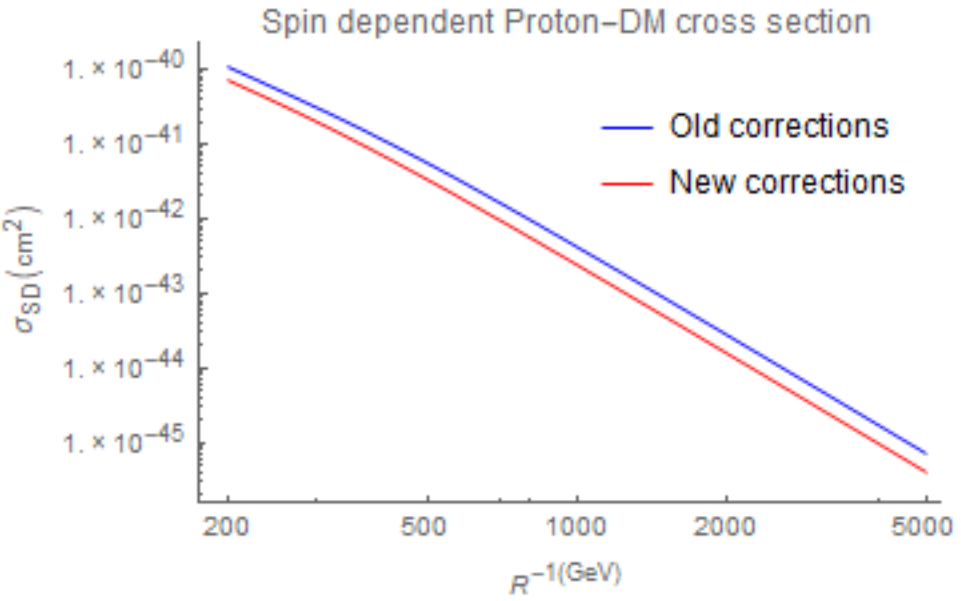

Figure 14: Comparision of the spin-dependent cross sections calculated using radiative correction from [17] (Old corrections) and [23] (New Corrections) respectively and $\Lambda R = 20$

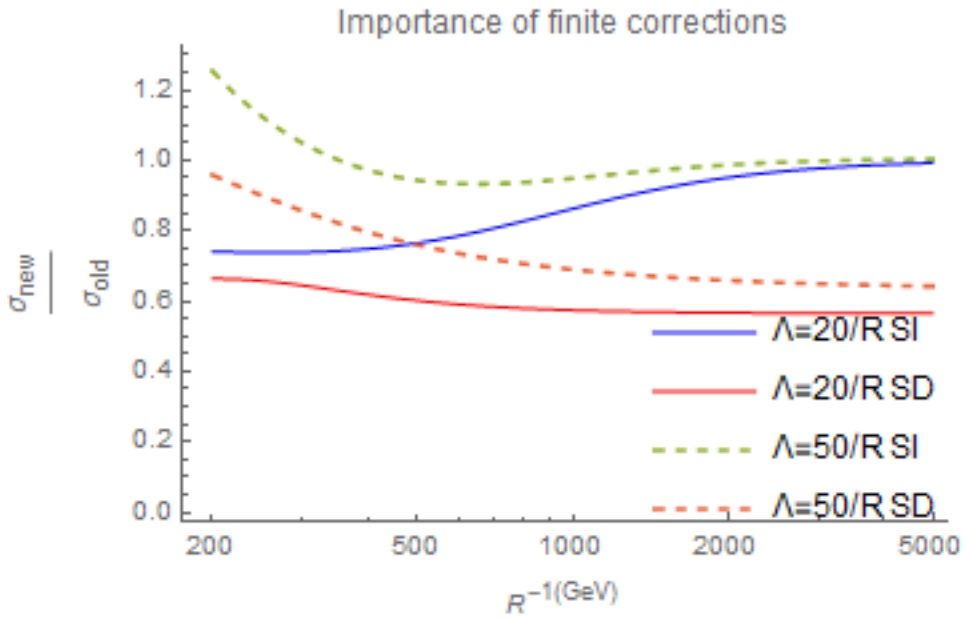

Figure 15: The ratio between the cross sections calculated using radiative correction from [23] (σ_{new}) and [17] (σ_{old}) for the spin-independent (SI) and spin-dependent (SD) cross sections

6 Discussion

6.1 The (m)UED parameter space

6.1.1 MUED parameters

In mUED there are only two free parameters the compactification scale R and the cut-off Λ. The compactification scale defines the size of the extra dimension, as discused in section 2.1. Making the extra dimension smaller means larger masses for KK-modes as well as larger mass splittings due to radiative corrections. As such The compactification scale is phenomenologically important and has a significant impact on direct detection. The standard model is non-renormailizable in higher dimensions. This means UED must be interpreted as an effective theory which is only valid up to a cut-off. In order to avoid regimes where the theory is strongly interacting one usually takes $\Lambda R < 50$ [12]. It has also been estimated that no new physics should appear before $\Lambda R \approx 20$ [5]. Radiative corrections depend on the cut-off meaning that it affects the masses of the theory and hence is phenomenologically significant. The radiative corrections to the KK-photon mass are small and hence the KK-photon mass is well approximated by R^{-1} .

Comparing the results found here with the limits from the Xenon-1T experiments [9] we find the spin dependent cross section are smaller than the 90 % confidence level for all values of $R^{-1} > 300$ GeV. In general the spin-dependent bounds are significantly weaker than the spin independent ones. The spin independent cross sections evade this bound for values of $R^{-1} > 450$ GeV for $\Lambda R = 20$ and $R^{-1} > 420$ GeV for $\Lambda R = 50$. As discussed briefly in the last section the

$B^{(1)} - B^{(1)} - H^{(0)}$ vertex used by Hissano et. al. [28] does not agree with the one given in other sources [48] [13], the latter being the related to the $\gamma^{(1)} - \gamma^{(1)} - H^{(0)}$ vertex used here. If we naively use the vertex from Hissano et. al. without worrying about the difference between $B^{(1)}$ and the photon we can estimate that the direct detection bound may be pushed up to $R^{-1} > 550$ GeV. The bound will in practice be smaller than this as the KK-photon vertex is slightly smaller than the $B^{(1)}$ vertex.

It has been estimated that mUED predicts the correct relic density in the range $1600 < R^{-1} < 1660$ GeV with the full set of radiative corrections when $\Lambda R = 20$ and $1630 < R^{-1} < 1785$ GeV [30]. This region of the parameter space is comfortably within the direct detection bounds.

6.1.2 Non-minimal theories

Non-minimal UED covers a large class of theories described by terms in the Lagrangian localized at the boundaries. For phenomenological purposes the whole class of non-minimal theories can be studied by treating the mass and couplings of every KK-particle as a free parameter. The most distinguishing feature of UED is the pseudo-degenerate spectrum of new particles. As such one would expect the mass splitting, i.e. the difference between the mass of the LKP and some other KK-particle, would be a parameter of interest.

While mUED unambiguously produces the KK-photon as the LKP, this is not necessarily the case in non-minimal theories. Here the LKP is assumed to be the KK-photon. Another candidate of interest would be the KK-neutrino. However direct detection seem to exclude this candidate as the lower bound on the WIMP mass would be around 50 TeV which does not seem to agree with the relic density calculation [48]. As the only KK-mass appearing in the cross sections are KK-quark masses the only mass splitting of interest will be $\Delta_q = \frac{m_{q^{(1)}} - m_{\gamma^{(1)}}}{m_{\gamma^{(1)}}}$ q being any quark.

The spin dependent cross sections are within the experimental bounds for all values of Δ_q so long as $R^{-1} > 1$ TeV. For the spin independent cross sections we found that increasing Δ_q above the mUED value reduces the cross sections for in the regimes where the KK-quark-exchange and gluon contributions dominate $R^{-1} < \mathcal{O}(TeV)$, but tend to saturate to a value close to the mUED cross section in the regime where the Higgs exchange dominates $R^{-1} > \mathcal{O}(TeV)$, as this contribution does not depend on any UED parameter except the KK-photon mass and weak mixing angle. When Δ_q is decreased below the mUED values for all KK-quarks except top-quark the cross sections increase, this gives us a lower bound of $\Delta_q = 0.025$ at the LHC bound decreasing to $\Delta_q = 0.015$ at $R^{-1} = 1800$ GeV. If instead we vary only one quark mass while keeping all others at the mUED value we find a similar effect.

Hence the mUED results for direct detection are robust and hold for any non-minimal extension unless said extension predicts a very small mass splitting compared to mUED.

6.2 Prospect of future detection

The next planed extension of the XENON1T experiment XENONnT is set to probe spin independent cross section as small as $2 \cdot 10^{-47}$ cm^2 [47] for WIMP-masses of 1 TeV. If we naively extrapolate this bound to larger WIMP masses we find the XENONnT may be able to probe mUED up to $R^{-1} \approx 1400$ GeV. While this is a significant improvement from the XENON1T bound the improvement over the current LHC bounds [11] of $R^{-1} > 1400$ GeV is marginal at best. Furthermore it will

not probe the region of mUED parameter-space favoured by the relic density. The mUED cross sections are however large enough to be detected by future experiments with higher sensitivity than XENONnT as they are larger than the neutrino floor up to approximately $R^{-1} \approx 2500\,\text{GeV}$. The neutrino floor refers to the fact that a sufficiently sensitive direct detection experiment will pick up signals from neutrinos interacting with the nuclei, and as such will have a hard challenge in subtracting the background [49]. As such all of the parameter space favoured by the relic density can in principle be tested by future direct detection experiments.

7 Conclusions

The goal of this thesis was to evaluate the direct detection cross section for the KK-photon and nucleons by calculating the relevant effective four-point couplings and implement them in DarkSUSY. These cross section were evaluated using the most recent radiative corrections [23] and the full leading order calculation of the gluon contribution.

The inclusion of the new radiative corrections reduces the cross sections significantly in regions where $R^{-1} < \mathcal{O}(TeV)$ which significantly reduces the lower bound on R^{-1} . With the help of the radiative corrections the lower bound on mUED is pushed down to $R^{-1} > 450\,\text{GeV}$. For non-minimal UED the same results hold unless the theory is made more degenerate by significantly reducing the quark masses. MUED, and by extension a large class of non-minimal theories, is still a viable solution to the dark matter problem and is not excluded by current direct detection bounds. The mUED cross section are in actually small enough that the KK-photon will likely evade detection by the upcoming XENONnT [47] experiment.

A Passarino-Veltmann reduction

When computing loop diagrams one has to integrate over a product of all propagators contain a loop momentum. As the box diagrams here contain 4 propagators these integrals will be of the form:

$$D0; D_\mu; D_{\mu\nu}; D_{\mu\nu\sigma}; D_{\mu\nu\sigma\rho}(p_1^2, p_2^2, p_3^2, m_1, m_2, m_3, m_4) \tag{94}$$
$$= \int \frac{d^4q}{i\pi^2} \frac{1; q_\mu; q_\mu q_\nu; q_\mu q_\nu q_\sigma; q_\mu q_\nu q_\sigma q_\rho}{(q^2 - m_1^2)((q+p_1)^2 - m_2^2)((q+p_1+p_2)^2 - m_3^2)((q+p_1+p_2+p_3)^2 - m_4^2)}$$

These integrals can be be reduced to scalar integrals, that is integrals without Lorentz indices [42] which have been calculated [52]. This approach called the Passarino-Veltmann reduction scheme [42] only works when the external momenta involved are independent, which is not the case as the two KK-photon momenta are equal. We therefore use an extended version of the Passarino-Veltmann reduction scheme implemented in LERG [50]. A similar approach was used for calculating the annihilation cross section of two KK-hypercharge bosons to two photons in [37], in fact the code used here is a modification of their program.

Focusing just on the denominator we can do a partial fraction decomposition to rewrite the four-point function in 94 as a combination of three-point functions

$$C0; C_\mu; C_{\mu\nu}; C_{\mu\nu\sigma}; C_{\mu\nu\sigma\rho}(p_1^2, p_2^2, (p_1+p_2)^2, m_1, m_2, m_3) = \int \frac{d^4q}{i\pi^2} \frac{1; q_\mu; q_\mu q_\nu; q_\mu q_\nu q_\sigma; q_\mu q_\nu q_\sigma q_\rho}{(q^2 - m_1^2)((q+p_1)^2 - m_2^2)((q+p_1+p_2)^2 - m_3^2)} \tag{95}$$

By being clever about the decomposition we can write the four-point functions which depend on momenta which are not independent in terms of a three or four three-point functions which depend on a set of independent momenta.

The necessary coefficients for calculating the cross sections can be separated into two different contributions the vector contribution and the pseudo-vector contribution. The vector contribution was found to be:

$$B1_v = \left(\frac{16}{(\eta+1)} + \frac{16\omega_g}{3m_{\gamma^{(1)}}(\eta+1)}\right)B0(4,0,0) - \left(\frac{16(2\eta+1)}{(\eta-1)} + \frac{8(13\eta+2)}{3m_{\gamma^{(1)}}(\eta-1)}\right)B0(4,\eta,\eta) \tag{96}$$

$$-\left(\frac{18\eta^4+22\eta^3-4\eta^2+8\eta-128}{3(\eta^2-1)} + \frac{4(-15\eta^4-13\eta^3+10\eta^2-4\eta+24)\omega_g}{3m_{\gamma^{(1)}}(\eta^2-1)}\right)B0(1+2\frac{\omega_g}{m_{\gamma^{(1)}}},0,\eta)$$

$$+\left(\frac{18\eta^4+22\eta^3+46\eta^2+56\eta-20}{3(\eta^2-1)} - \frac{4(15\eta^4+48\eta^3-9\eta^2+18\eta-28)\omega_g}{3m_{\gamma^{(1)}}(\eta^2-1)}\right)B0(0,\eta,\eta)$$

$$+\left(\frac{32\eta(\eta+2)}{(\eta-1)} + \frac{16\eta(4+\eta)\omega_g}{m_{\gamma^{(1)}}(\eta-1)}\right)C0(4,0,0,\eta,\eta,\eta) + \frac{32}{\eta-1}C0(1,0,1+2\frac{\omega_g}{m_{\gamma^{(1)}}},0,\eta,\eta)$$

$$+\frac{2(-226-72\eta-75\eta^2+42\eta^3+27\eta^4)}{9(\eta^2-1)} - \frac{4(-20+18\eta-9\eta^2+48\eta^3+45\eta^4)\omega_g}{9m_{\gamma^{(1)}}(\eta^2-1)}$$

$$B2_v = \left(\frac{40}{3(\eta+1)} + \frac{8\omega_g}{m_{\gamma^{(1)}}(\eta+1)}\right)B0(4,0,0) - \left(\frac{20(\eta+2)}{3(\eta-1)} + \frac{8(\eta+1)\omega_g}{m_{\gamma^{(1)}}(\eta-1)}\right)B0(4,\eta,\eta)) \tag{97}$$

$$-\left(\frac{4(3\eta^4+5\eta^3+\eta-25)}{3(\eta^2-1)} - \frac{8(3\eta^4-\eta^3+2\eta^2+5\eta-11)\omega}{3m_{\gamma^{(1)}}(\eta^2-1)}\right)B0\left(1+2\frac{\omega_g}{m_{\gamma^{(1)}}},0,\eta\right)$$

$$+\left(\frac{4(3\eta^4+5\eta^3+5\eta^2+9\eta-8)}{3(\eta^2-1)} - \frac{8(3\eta^4-\eta^3-\eta^2-\eta-14)\omega_g}{3m_{\gamma^{(1)}}(\eta^2-1)}\right)B0(0,\eta,\eta)$$

$$+\left(\frac{8\eta(\eta+4)}{\eta-1} + \frac{32\eta\omega_g}{m_{\gamma^{(1)}}(\eta-1)}\right)C0(4,0,0,\eta,\eta,\eta) - \frac{8\eta}{\eta-1}C0\left(1,0,1+2\frac{\omega_g}{m_{\gamma^{(1)}}},0,\eta,\eta\right) - \frac{64\omega_g}{3m_{\gamma^{(1)}}(\eta^2-1)} - \frac{4(1+30\eta+2\eta^2+3\eta^3)}{3\eta(\eta^2-1)}$$

$$+\frac{4(-1-39\eta-6\eta^3+5\eta^4+3\eta^5)}{3\eta(\eta^2-1)} - \frac{8(-1+6\eta-\eta^2-\eta^3+\eta^4)\omega}{3m_{\gamma^{(1)}}(\eta^2-1)}$$

..

$$B6 = (\frac{28}{3(\eta+1)} + \frac{4\omega_g}{m_{\gamma(1)}(\eta+1)})B0(4,0,0) - (\frac{28+26\eta}{3(\eta-1)} + \frac{(13\eta+4)\omega}{m_{\gamma(1)}(\eta-1)})B0(4,\eta,\eta) \tag{98}$$

$$-(\frac{2(-44+28\eta-2\eta^2-13\eta^3+9\eta^4)}{3(\eta^2-1)} - \frac{4(-24+28\eta-10\eta^2-11\eta^3+15\eta^4)\omega}{3m_{\gamma(1)}(\eta^2-1)}B(1+2\frac{\omega_g}{m_{\gamma(1)}},0,\eta)$$

$$+(\frac{18\eta^4-26\eta^3+22\eta^2+90\eta-40}{3(\eta^2-1)} - \frac{60\eta^4-44\eta^3+118\eta^2+22\eta-108)\omega_g}{3m_{\gamma(1)}(\eta^2-1)})B0(0,\eta,\eta)$$

$$+\frac{4\eta(\eta+8)}{\eta-1}+)\frac{12\eta(\eta+4)\omega_g}{m_{\gamma(1)}(\eta-1)}C0(4,0,0,\eta,\eta,\eta) - 16C0(1,0,1+2\frac{\omega_g}{m_{\gamma(1)}},0,\eta,\eta)$$

$$+\frac{(2(-178+63\eta-12\eta^2-30\eta^3+27\eta^4)}{9(\eta^2-1)} - \frac{2(-22+57\eta-9\eta^2-16\eta^3+30\eta^4)\omega_g}{3(\eta^2-1)m_{\gamma(1)}}$$

The pseudovector contribution was found to be:

$$B1_a = B1_v - 32\eta((1-2\frac{\omega}{m_{\gamma(1)}})(B0(1+2\frac{\omega}{m_{\gamma(1)}},0,\eta) - B0(0,\eta,\eta) - 1) \tag{99}$$

$$B2_a = B2_v + 32\eta((1-2\frac{\omega}{m_{\gamma(1)}})(B0(1+2\frac{\omega}{m_{\gamma(1)}},0,\eta) - B0(0,\eta,\eta) - 1) \tag{100}$$

where $\eta = \frac{m_k q^2}{m^2_{\gamma(1)}}$.

The two-point and three-point are all given in Bergstöm et. al. [37] except $B0(1+\frac{2\omega_g}{m_{\gamma(1)}},0,\eta)$ and $C0(1,0,1+\frac{2\omega_g}{m_{\gamma(1)}},0,\eta,\eta)$ These were found to be:

$$B0(1+\frac{2\omega_g}{m_{\gamma(1)}},0,\eta) = -\frac{(2+4\frac{\omega_g}{M}) - \eta\ln(\eta) + (\eta-1+2\frac{\omega_g}{M})\ln\left(\eta-1-2\frac{\omega_g}{M}\right)}{1+2\frac{\omega_g}{M}} \tag{101}$$

$$C0(1,0,1+2\frac{\omega_g}{m_{\gamma(1)}},0,\eta,\eta) = \int \frac{d^4q}{(2\pi)^4}\frac{1}{q^2((q+p)^2+m^2_{q(1)})((q+p+p_3)^2+m^2_{q(1)})} \tag{102}$$

$$= \int \frac{d^4q}{(2\pi)^4}\frac{1}{(q^2+m^2_{q(1)})(q+p_3^2+m^2_{q(1)})(q-p)^2} = \int_0^1 dx\int_0^x dy(2y(\omega+x+x\omega)+(1+2\omega)x^2+x(\eta+1+2\omega)-i\epsilon)^{-1} \tag{103}$$

where $\omega = \frac{\omega_g}{m_{\gamma(1)}}$

In the last step using 5.2 from 't Hooft Veltman [52] with

$$a = 1+2\omega \;\; b = 0 \;\; c = 2+2\omega \;\; d = \eta+1+2\omega \;\; e = 2\omega \;\; f = -i\epsilon \tag{104}$$

$$C0(1,0,1+2\frac{\omega_g}{M},0,\eta,\eta) = -\int_0^1 dx \frac{\ln\left(x+\frac{x^2(1+2\omega)+x(1+\eta+2\omega)-i\epsilon}{2(x\omega+x+\omega)}\right)-\ln\left(\frac{x^2(1+2\omega)+x(1+\eta+2\omega)-i\epsilon}{2(x\omega+x+\omega)}\right)}{2(x\omega+x+\omega)} \quad (105)$$

$$= \int_0^1 dx \frac{\ln\left(\frac{x^2(1+2\omega)+x(1+\eta+2\omega)+2x(x\omega+x+\omega)-i\epsilon}{x^2(1+2\omega)+x(1+\eta+2\omega)-i\epsilon}\right)}{2(x\omega+x+\omega)}$$

$$= \int_0^1 dx \frac{\ln\left(\frac{(3+4\omega)x+(1+\eta+4\omega)}{(1+2\omega)x+(1+\eta+2\omega)}\right)}{2(x\omega+x+\omega)} \quad (106)$$

$$= \int_0^1 dx \frac{\ln((3+4\omega)x+(1+\eta+4\omega))-\ln(x(1+2\omega)+(1+\eta+2\omega))}{2(x\omega+x+\omega)} \quad (107)$$

to frist order in $\frac{\omega_g}{m_{\gamma(1)}}$

$$\approx \frac{1}{2}(-\ln(3)\ln(1+\eta)-\ln\left(\frac{-1}{1+\eta}\right)\ln(2+\eta)+\ln(3)\ln(4+\eta)+\ln\left(\frac{-1}{1+\eta}\right)-Li_2(\frac{2+\eta}{1+\eta})+Li_2(\frac{4+\eta}{1+\eta}) \quad (108)$$

$$\frac{\omega_g}{2m_{\gamma(1)}}(-\frac{4\ln(3)}{1+\eta}+\frac{8\ln(3)}{4+\eta}+\frac{2\ln(-\eta-1)}{1+\eta}-\frac{(4+7\eta)\ln\left(\frac{-3}{1+\eta}\right)}{(1+\eta)(4+\eta)}-\frac{4\ln\left(\frac{-1}{1+\eta}\right)}{2+\eta}+\frac{8\ln\left(\frac{-1}{1+\eta}\right)}{4+\eta}) \quad (109)$$

$$\frac{\omega_g}{2m_{\gamma(1)}}(\frac{(2+3\eta)\ln\left(\frac{-1}{1+\eta}\right)}{(1+\eta)(2+\eta)}+\ln(1+\eta)(\frac{2}{3}+\ln(3))+\ln(2+\eta)(\ln\left(\frac{-1}{1+\eta}\right)+\frac{\eta}{1+\eta}-2)+\ln(4+\eta)(\frac{4}{3}+\frac{\eta}{1+\eta}) \quad (110)$$

$$\frac{\omega_g}{2m_{\gamma(1)}}(-\ln(3)+\ln\left(\frac{-1}{1+\eta}\right)\frac{\ln\left(\frac{-3}{1+\eta}\right)+\ln\left(\frac{-1}{1+\eta}\right)-4}{1+\eta}+Li_2(\frac{2+\eta}{1+\eta})-Li_2(\frac{4+\eta}{1+\eta})) \quad (111)$$

where the Spence function or dilogarithm is defined as:

$$Li_2(z) = -\int_0^1 dx \frac{\ln(1-zx)}{x} = \sum_{k=1}^{\infty}\frac{z^k}{k^2} \quad (112)$$

References

[1] Adams, D., Adeva, B., Arik, E., Arvidson, A., Badelek, B., Ballintijn, M., Bardin, G., Baum, G., Berglund, P., Betev, L., et al. (1995). A new measurement of the spin-dependent structure function g1 (x) of the deuteron. *Physics Letters B*, 357(1-2):248–254.

[2] Aghanim, N., Akrami, Y., Ashdown, M., Aumont, J., Baccigalupi, C., Ballardini, M., Banday, A., Barreiro, R., Bartolo, N., Basak, S., et al. (2018). Planck 2018 results. *arXiv preprint arXiv:1807.06209*.

[3] Amole, C., Ardid, M., Asner, D. M., Baxter, D., Behnke, E., Bhattacharjee, P., Borsodi, H., Bou-Cabo, M., Brice, S., Broemmelsiek, D., et al. (2016). Dark matter search results from the pico-60 cf 3 i bubble chamber. *Physical Review D*, 93(5):052014.

[4] Appelquist, T., Cheng, H.-C., and Dobrescu, B. A. (2001a). Bounds on universal extra dimensions. *Physical Review D*, 64(3):035002.

[5] Appelquist, T., Dobrescu, B. A., Ponton, E., and Yee, H.-U. (2001b). Proton stability in six dimensions. *Physical Review Letters*, 87(18):181802.

[6] Armour, K., Bowen, M., Ellis, S., and Strassler, M. (2004). Analytic parameterizations of parton distribution functions. *unpublished work*.

[7] Barger, V., Keung, W.-Y., and Shaughnessy, G. (2008). Spin dependence of dark matter scattering. *Physical Review D*, 78(5):056007.

[8] Belanger, G., Kakizaki, M., and Pukhov, A. (2011). Dark matter in ued: the role of the second kk level. *Journal of Cosmology and Astroparticle Physics*, 2011(02):009.

[9] Benabderrahmane, M. (2019). Latest results from the xenon1t experiment. In *Journal of Physics: Conference Series*, volume 1258, page 012009. IOP Publishing.

[10] Benoit, A., Bergé, L., Bluemer, J., Broniatowski, A., Censier, B., Chabert, L., Chapellier, M., Chardin, G., Collin, S., De Jesus, M., et al. (2005). Sensitivity of the edelweiss wimp search to spin-dependent interactions. *Physics Letters B*, 616(1-2):25–30.

[11] Beuria, J., Datta, A., Debnath, D., and Matchev, K. T. (2018). LHC Collider Phenomenology of Minimal Universal Extra Dimensions. *Comput. Phys. Commun.*, 226:187–205.

[12] Bhattacharya, G., Majee, S., and Datta, A. (2006). Power law blitzkrieg in universal extra dimension scenario. *Nucl. Phys. B*, 760(hep-ph/0608208):117–127.

[13] Bringmann, T. (2005). *Cosmological aspects of universal extra dimensions*.

[14] Bringmann, T., Edsjö, J., Gondolo, P., Ullio, P., and Bergström, L. (2018). Darksusy 6: an advanced tool to compute dark matter properties numerically. *Journal of Cosmology and Astroparticle Physics*, 2018(07):033.

[15] Carroll, S. M. (2019). *Spacetime and geometry*. Cambridge University Press.

[16] Cerdeno, D. G. and Green, A. M. (2010). Direct detection of wimps. *arXiv preprint arXiv:1002.1912*.

[17] Cheng, H.-C., Matchev, K. T., and Schmaltz, M. (2002). Radiative corrections to kaluza-klein masses. *Physical Review D*, 66(3):036005.

[18] Dodelson, S. and Liguori, M. (2006). Can cosmic structure form without dark matter? *Phys. Rev. Lett.*, 97:231301.

[19] Edsjo, J. (1997). Aspects of neutrino detection of neutralino dark matter. *arXiv preprint hep-ph/9704384*.

[20] Eidelman, S., Hayes, K., Olive, K. e., Aguilar-Benitez, M., Amsler, C., Asner, D., Babu, K., Barnett, R., Beringer, J., Burchat, P., et al. (2004). Review of particle physics. *Physics letters B*, 592(1-4):1–5.

[21] Fan, J., Reece, M., and Wang, L.-T. (2010). Non-relativistic effective theory of dark matter direct detection. *Journal of Cosmology and Astroparticle Physics*, 2010(11):042.

[22] Fitzpatrick, A. L., Haxton, W., Katz, E., Lubbers, N., and Xu, Y. (2013). The effective field theory of dark matter direct detection. *Journal of Cosmology and Astroparticle Physics*, 2013(02):004.

[23] Freitas, A., Kong, K., and Wiegand, D. (2018). Radiative corrections to masses and couplings in universal extra dimensions. *Journal of High Energy Physics*, 2018(3):93.

[24] G.Belanger, F.Boudjema, A. and A.Semenov (2008). Dark matter direct detction rates in a generic model with micromega$_2$.2.

[25] Georgi, H., Grant, A. K., and Hailu, G. (2001). Brane couplings from bulk loops. *Physics Letters B*, 506(1-2):207–214.

[26] Hisano, J., Ishiwata, K., and Nagata, N. (2010). Gluon contribution to dark matter direct detection. *Physical Review D*, 82(11):115007.

[27] Hisano, J., Ishiwata, K., Nagata, N., and Yamanaka, M. (2011). Direct detection of vector dark matter. *Progress of Theoretical Physics*, 126(3):435–456.

[28] Hisano, J., Nagata, K. I. N., , and Yamanaka, M. (2015). Direct detection of vector dark matter.

[29] Hoyle, C. D., Schmidt, U., Heckel, B. R., Adelberger, E. G., Gundlach, J. H., Kapner, D. J., and Swanson, H. E. (2001). Submillimeter test of the gravitational inverse-square law: A search for "large" extra dimensions. *Phys. Rev. Lett.*, 86:1418–1421.

[30] Jacobsen, S. (2019). Relic density of kaluza-klein dark matter. Master's thesis.

[31] Jungman, G., Kamionkowski, M., and Griest, K. (1996a). Supersymmetric dark matter. *Physics Reports*, 267(5-6):195–373.

[32] Jungman, G., Kamionkowski, M., and Griest, K. (1996b). Supersymmetric dark matter. *Physics Reports*, 267(5-6):195–373.

[33] Kaluza, T. (1921). Zum unitätsproblem der physik. *Int. J. Mod. Phys.*, 1921(arXiv: 1803.08616):1870001.

[34] Kavanagh, B. J. and O'Hare, C. A. J. (2016). Reconstructing the three-dimensional local dark matter velocity distribution. *Phys. Rev. D*, 94:123009.

[35] Klein, O. (1926). Quantentheorie und fünfdimensionale relativitätstheorie. *Zeitschrift für Physik*, 37(12):895–906.

[36] Koopmans, L., Auger, M., Barnabe, M., Bolton, A., Bradac, M., Ciotti, L., Congdon, A., Czoske, O., Dye, S., Dutton, A., et al. (2009). Strong gravitational lensing as a probe of gravity, dark-matter and super-massive black holes. *arXiv preprint arXiv:0902.3186*.

[37] L.Bergstro¨m, T. Bringmann, M. E. and M.Gustafsson (2005). Two photon annihilation of kaluza-klein dark matter.

[38] Liu, J., Chen, X., and Ji, X. (2017). Current status of direct dark matter detection experiments. *Nature Physics*, 13(3):212–216.

[39] M.Peskin and D.Schroeder (1995). *An introduction to quantum field theory*. Westview Press.

[40] Nielsen, H. B. and Rugh, S. E. (1993). Why do we live in (3+1)-dimensions? In *Proceedings, 26th International Ahrenshoop Symposium on the Theory of Elementary Particles: Wendisch-Rietz, Germany, September 9-13, 1992*, pages 307–337.

[41] Ohki, H., Fukaya, H., Hashimoto, S., Kaneko, T., Matsufuru, H., Noaki, J., Onogi, T., Shintani, E., Yamada, N., Collaboration, J., et al. (2008). Nucleon sigma term and strange quark content from lattice qcd with exact chiral symmetry. *Physical Review D*, 78(5):054502.

[42] Passarino, G. and Veltman, M. (1979). One-loop corrections for e+ e- annihilation into μ+ μ- in the weinberg model. *Nuclear Physics B*, 160(1):151–207.

[43] Pizagno, J., Prada, F., Weinberg, D. H., Rix, H.-W., Harbeck, D., Grebel, E. K., Bell, E. F., Brinkmann, J., Holtzman, J., and West, A. (2005). Dark matter and stellar mass in the luminous regions of disk galaxies. *The Astrophysical Journal*, 633(2):844.

[44] Pumplin, J., Stump, D. R., Huston, J., Lai, H.-L., Nadolsky, P., and Tung, W.-K. (2002). New generation of parton distributions with uncertainties from global qcd analysis. *Journal of High Energy Physics*, 2002(07):012.

[45] Rohatgi, A. (2019). Webplotdigitizer 4.2.

[46] Rubin, V. C. and Ford Jr, W. K. (1970). Rotation of the andromeda nebula from a spectroscopic survey of emission regions. *The Astrophysical Journal*, 159:379.

[47] Selvi, D. M., Garbini, D. M., and Corasaniti, M. (2016). Monte carlo simulation of a neutron veto for the xenonnt experiment.

[48] Servant, G. and Tait, T. M. (2002). Elastic scattering and direct detection of kaluza-klein dark matter. *New Journal of Physics*, 4(1):99.

[49] Strege, C., Trotta, R., Bertone, G., Peter, A. H. G., and Scott, P. (2012). Fundamental statistical limitations of future dark matter direct detection experiments. *Phys. Rev. D*, 86:023507.

[50] Stuart, R. G. (1995). Algebraic reduction of feynman diagrams to scalar integrals: A mathematica implementation of lerg-i. *Computer physics communications*, 85(2):267–277.

[51] T. Bringmann, S. H. (2016). Thermal decoupling of wimps from first principles.

[52] t Hooft, G. and Veltman, M. (1979). Scalar one-loop integrals. *Nuclear Physics B*, 153:365–401.

[53] Van Ritbergen, T., Schellekens, A., and Vermaseren, J. (1999). Group theory factors for feynman diagrams. *International Journal of Modern Physics A*, 14(01):41–96.

[54] Young, R. and Thomas, A. (2010). Octet baryon masses and sigma terms from an su (3) chiral extrapolation. *Physical Review D*, 81(1):014503.